References

Agnes, G.S. 1997. Performance of nonlinear mechanical, resonant-shunted piezoelectric, and electronic vibration absorbers for multi-degree-of-freedom structures. *PhD Thesis*, Virginia Polytechnic Institute and State University.

Braun, D. 1980. Development of anti-resonance force isolators for helicopter vibration reduction, *Sixth European rotorcraft and powered lift aircraft forum*, Bristol, England, September 16-19.

Braun, D. 1988. Vibration isolator particularly of the anti-resonance type. *U.S. Patent 4,781,363.*

Brock, J.E. 1946. A note on the damped vibration absorber. *Transactions of the American Society of Mechanical Engineers A*, 284.

Davey, A.B., Payne, A.R. 1964. *Rubber in engineering practice*. London: Applied Science Publishers.

Den Hartog, J.P. 1956. *Mechanical vibrations*, Fourth Edition, New-York: McGraw-Hill.

Desanghere, G. & Vansevenant, E. 1991. An adaptive tuned vibration absorber, *Proceedings of the 10th IMAC*, p.1347-1352.

Desjardins, R.A. & Hooper W.E. 1980. Antiresonant rotor isolation for vibration reduction, *Journal of the American Helicopter Society*, Vol. 25, no. 3, July, p.46-55.

Desjardins, R.A. & Hooper, W.E. 1976. Rotor isolation of the hingeless rotor B0-105 and YUH-61A helicopters, *2nd European Rotorcraft and Powered Lift Aircraft Forum*, Buckeburg, F.R.G., September.

Desjardins, R.A., Ellis, C.W. & Sankewitsch, V. 1978. Vibration isolation system. *U.S. patent no. 4,088,042.*

Desjardins, R.A., & Sankewitsch, V. 1982. Vibration isolation system. *U.S. patent no. 4,311,213.*

Dumbaugh, G.D. 1984. The evolution of the first "universal" vibratory drive system for moving and processing bulk solid materials, *Bulk Solids Handling*, vol. 4, no. 1, March, p.125-140.

Ewins, D.J. 1995. *Modal testing: theory and practice*, Baldock: Research Studies Press.

Fischer, P., Karrer, H., Kamla, T. 1998. Tuning of vibration absorbers under wide band excitation by stochastic dynamic analysis, International conference on noise and vibration engineering, September 16-18.

Flannely, W.G. 1966. The dynamic anti-resonant vibration isolator. *22nd Annual AHS National Forum*, Washington, p.152-158.

Frahm, H. 1909. Device for damping vibrations of bodies, *U.S. Patent no. 989958.*

Franchek, M.A., Ryan, M.W. & Bernhard, R.J. 1995, Adaptive passive vibration control, *Journal of Sound and Vibration*, 189(5), p.565-585.

Frolov, K., Goncharevich, I. 1991. *Vibration technology theory and practice*. Boca Raton: CRC Press.

Gaffey, T.M. & Balke, R.W. 1976. Isolation of rotor induced vibration with the Bell focal pylon-nodal beam system. *Society of Automotive Engineers*. p.1-10.

Garibaldi, L. & Onah, H.N. 1996. *Viscoelastic material damping technology*, Torino: Becchis Osiride.

Gere, J.M. & Tomoshenko, S.P. 1991, *Mechanics of materials*. London: Chapman & Hall.

Greenway, M. 1983. Vibration in screening plants: designing out maintenance, *Proceedings of the 1983 Maintenance Management Convention*, October 17-19.

Halwes, D.R. et al., 1980. *Vibration suppression system, U.S. patent no. 4,236,607.*

Halwes, D.R., 1981. Total main rotor isolation system analysis, Bell Helicopter Textron, *NASA Contractor Report No. 165667*. Langley Research Center, Hampton, Virginia, June.

Heyns, P.S. & Van Niekerk, J.L. 1997. Vibrating screen technology: An overview of vibration control methods. LGI Report no LGI97/075.

Igusa, T. & Xu, K. 1991. Vibration reduction characteristics of distributed tuned mass dampers, *Proceedings of the 4th International Conference on Structural Dynamics: Recent Advances*, Southampton, 15-18 July, p.596-605.

ISO 7626. *Methods for the experimental determination of mechanical mobility*.

Johnson, D.A. 1991. Optimal dynamic absorber for transients - Application to the motion of a robot arm, *Proceedings of the 9th IMAC*.

Korenev, B.G. & Reznikov L.M., 1993. *Dynamic vibration absorbers theory and technical applications*, West Sussex: Wiley.

Mackie, K., Marais, C. & Heyns, M. 1997. The dynamic characteristics of type AB Neidhart systems. *LGI report no. 97/038*.

Maia, N.M.M. & Júlio, M.M.S. (Editors) 1998. *Theoretical and experimental modal analysis*. Baldock: Research Studies Press.

Margolis, D.L. & Baker, D. 1992. The variable fulcrum isolator: A low power, nonlinear, vibration control component. *Transactions of the ASME*, March, Vol. 114, p.148-154.

Nashif, A.D., Jones, D.I.G., Henderson, J.P. 1985. *Vibration damping,* New York: John Wiley & Sons.

O'Leary, J.J. 1969. Reduction in the vibration of the CH-47C helicopter using a variable tuning vibration absorber, *Shock and vibration symposium*, December.

Olgac, N. & Holm-Hansen, B.T. 1993. Vibration absorbers utilizing only position measurements for time varying excitation frequencies. *ASME Symposium on Mechatronics*.

Patankar, S.V. 1980. *Numerical heat transfer and fluid flow*, New York: McGraw-Hill.

Rao S.S. 1990. *Mechanical vibrations*, 2nd Edition, New York: Addison Wesley.

Rice, H.J. 1987. Stable design of asymmetric non-linear vibration absorbers. *Proceedings of the 5th IMAC*. p.1474-1478.

Riddle, T., Bates, G. & Thomas, G. 1984. Summary report on the design on nine isolation system subframes systems, *Structural Dynamics Research Corporation*, Ohio: SDRC.

Rita, A.D., McGarvey, J.H., Jones, R. 1976. Helicopter rotor isolation utilizing the dynamic antiresonant vibration isolator, *32nd Annual AHS National Forum*, Washington, May.

Shaw C.T. 1992. *Using computational fluid dynamics*, Englewood Cliffs: Prentice Hall.

Smith, M.R. & Stamps, F.N. 1988. Vibration isolation system, *US patent no. 5,788,029.*

Tsai, H.-C. & Lin, G.-C. 1994. Explicit formulae for optimum absorber parameters for force excited and viscously damped systems, *Journal of Sound and Vibration,* 176(5), p.585-596.

White, F.M. 1991. *Viscous fluid flow*, 2nd Edition, McGraw-Hill.

White, F.M. 1988. *Fluid Mechanics*, 2nd Edition, McGraw-Hill.

APPENDIX A

Mathematical model of a single D.O.F vibration absorber

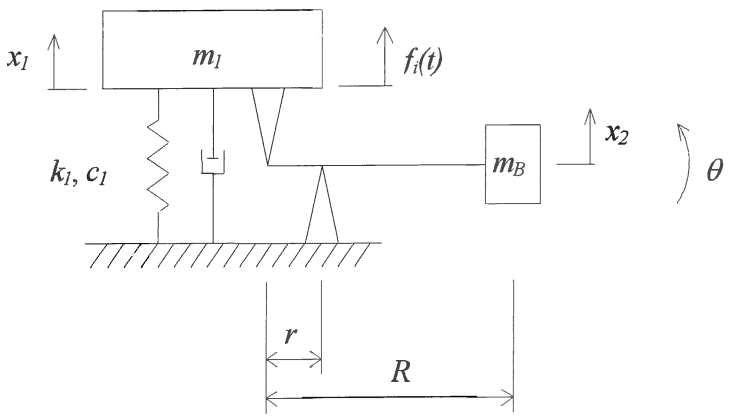

Figure A.1 A single D.O.F. vibration absorber system

The kinetic energy of the system in figure A.1 is given by equation A.1:

$$T = \frac{1}{2}\left(m_1\dot{x}_1^2 + m_B\dot{x}_2^2 + I_G\dot{\theta}^2\right) \qquad \textbf{(A.1)}$$

I_G is the moment of inertia of the mass m_B about its mass centre. The relation between x_3, θ, and x_2 are given by equations A.2 and A.3 (refer to figure A.2):

$$x_2 = \left(1 - \frac{R}{r}\right)x_1 \qquad \textbf{(A.2)}$$

$$\theta \approx -\frac{x_1}{r} \qquad \textbf{(A.3)}$$

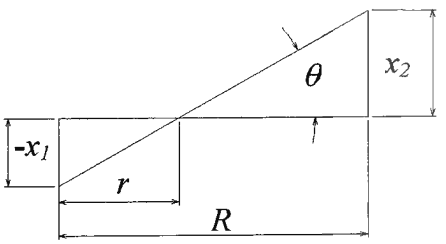

Figure A.2 Schematic of relationship between the variables

Substituting these relations in equation A.1 results in the following:

$$T = \frac{1}{2}\left(m_1 + \left(1 - \frac{R}{r}\right)^2 m_B + \frac{I_G}{r^2}\right)\dot{x}_1^2 \qquad \textbf{(A.4)}$$

From equation A.4 the kinetic term in the Lagrange's equations can be derived:

$$\frac{d}{dt}\left(\frac{\partial T}{\partial \dot{x}_1}\right) = \left(m_1 + \left(1-\frac{R}{r}\right)^2 m_B + \frac{I_G}{r^2}\right)\ddot{x}_1 \tag{A.5}$$

The elastic energy is given by:

$$V = \frac{1}{2}k_1 x_1^2 \tag{A.6}$$

From equation A.6 the potential energy term in the Lagrange's equations can be derived:

$$\frac{\partial V}{\partial x_1} = k_1 x_1 \tag{A.7}$$

The Rayleigh function is given by:

$$R = \frac{1}{2}c_1 \dot{x}_1^2 \tag{A.8}$$

From equation A.8 the damping term in the Lagrange's equations can be derived:

$$\frac{\partial R}{\partial \dot{x}_1} = c_1 \dot{x}_1 \tag{A.9}$$

The complete equation of motion (A.11) can be formulated by substituting the expressions in Lagrange's equations (A.10) with those found in equations A.5, A.7 and A.9.

$$\frac{d}{dt}\left(\frac{\partial T}{\partial \dot{x}_j}\right) - \frac{\partial T}{\partial x_j} + \frac{\partial V}{\partial x_j} = Q_j^{(n)} \qquad j = 1,2,\ldots,n \tag{A.10}$$

$$\left(m_1 + m_B\left(1-\frac{R}{r}\right)^2 + \frac{I_G}{r^2}\right)\ddot{x}_1 + c_1\dot{x}_1 + k_1 x_1 = F_0 \sin(\omega t) \tag{A.11}$$

The frequency response of the system to a force can be found by substituting the assumed solution and its derivatives (A.12, A.13 and A.14) as well as the harmonic force (A.15) into the equation motion (A.11). The frequency response to a force $F_j(i\omega)$ is shown in equation A.16.

$$x_j(t) = X_j e^{i\omega t} \tag{A.12}$$

$$\dot{x}_j(t) = i\omega X_j e^{i\omega t} \tag{A.13}$$

$$\ddot{x}_j(t) = -\omega^2 X_j e^{i\omega t} \tag{A.14}$$

$$f_j(t) = F_j e^{i\omega t} \tag{A.15}$$

$$X_1 = \frac{1}{-\omega^2\left[m_1 + m_B\left(1-\frac{R}{r}\right)^2 + \frac{I_G}{r^2}\right] + i\omega c_1 + k_1} F_1 \tag{A.16}$$

The transmissibility will be defined in terms of forces. For this purpose the force transmitted by the spring (F_v), the damper (F_d) and the dynamic force of the absorber (F_a) must be calculated. The first two are simply given by equation A.17 and A.18:

$$F_v = k_1 x_1 \tag{A.17}$$

$$F_d = c_1 \dot{x}_1 \tag{A.18}$$

The complete derivation of equation A.19 is shown in Appendix D.

$$F_a = -\left[m_B \left(1 - \frac{R}{r} \right) \frac{R}{r} - \frac{I_G}{r^2} \right] \ddot{x}_1 \tag{A.19}$$

The transmissibility is given in terms of the forces and as a function of frequency. Equations A.17 to A.19 are rewritten using equations A.12 to A.14 and added to arrive at the total force transmitted to the foundation. The force applied at mass m_1 is given by equation A.15. The transmissibility is therefore:

$$\begin{aligned} \frac{F_o}{F_i} &= \frac{\left[k_1 + i\omega c_1 + \omega^2 \left(m_B \left(1 - \frac{R}{r} \right) \frac{R}{r} - \frac{I_G}{r^2} \right) \right] X_1}{F_1} \\ &= \frac{k_1 + i\omega c_1 + \omega^2 \left[m_B \left(1 - \frac{R}{r} \right) \frac{R}{r} - \frac{I_G}{r^2} \right]}{k_1 + i\omega c_1 - \omega^2 \left[m_1 + m_B \left(1 - \frac{R}{r} \right)^2 + \frac{I_G}{r^2} \right]} \end{aligned} \tag{A.20}$$

Equation A.20 can be non-dimensionalised as follows:

$$|T_r| = \left\{ \frac{\left[1 - \left(\frac{\omega}{\omega_a} \right)^2 \right]^2 + \left[2\zeta \frac{\omega}{\omega_n} \right]^2}{\left[1 - \left(\frac{\omega}{\omega_n} \right)^2 \right]^2 + \left[2\zeta \frac{\omega}{\omega_n} \right]^2} \right\}^{\frac{1}{2}} \tag{A.21}$$

$$\phi = \tan^{-1} \left\{ \frac{2\zeta \frac{\omega}{\omega_n}}{1 - \left(\frac{\omega}{\omega_a} \right)^2} \right\} - \tan^{-1} \left\{ \frac{2\zeta \frac{\omega}{\omega_n}}{1 - \left(\frac{\omega}{\omega_n} \right)^2} \right\} \tag{A.22}$$

The following transmissibility plot of equation A.20 illustrates the effect of damping. The importance of low damping in the absorber is clearly evident.

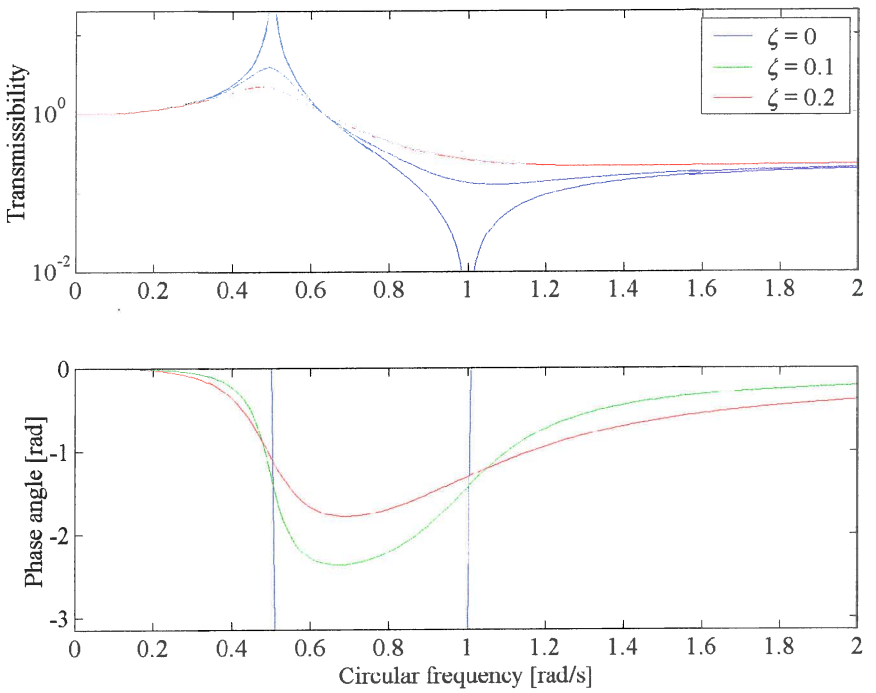

Figure A.3 Transmissibility plot of equation A.20 with $\omega_a = 1$, $\omega_n = 0.5$

The aim of the absorber is to minimise the force transferred to the foundation. This will be achieved when the numerator in the transmissibility equation (A.20) is equal to zero:

$$k_1 + i\omega c_1 + \omega^2\left[m_B\left(1-\frac{R}{r}\right)\frac{R}{r} - \frac{I_G}{r^2}\right] = 0 \qquad \textbf{(A.21)}$$

The non-trivial solution for the isolation frequency ($c_1 = 0$) is:

$$f_a = \frac{1}{2\pi}\sqrt{\frac{-k_1}{m_B\left(1-\frac{R}{r}\right)\frac{R}{r} - \frac{I_G}{r^2}}} \qquad \textbf{(A.22)}$$

The response of the screen to the applied force after the addition of the absorber is of critical importance since it will influence its effective operation. The response of the screen is given by equation A.16. From this equation it is evident that the response of the screen will be influenced by the addition of an absorber. The effect must be minimised through proper choice of parameters and the applied force must be adjusted to compensate.

The following figure illustrates the forced response of the system. The response at the isolation frequency can be low.

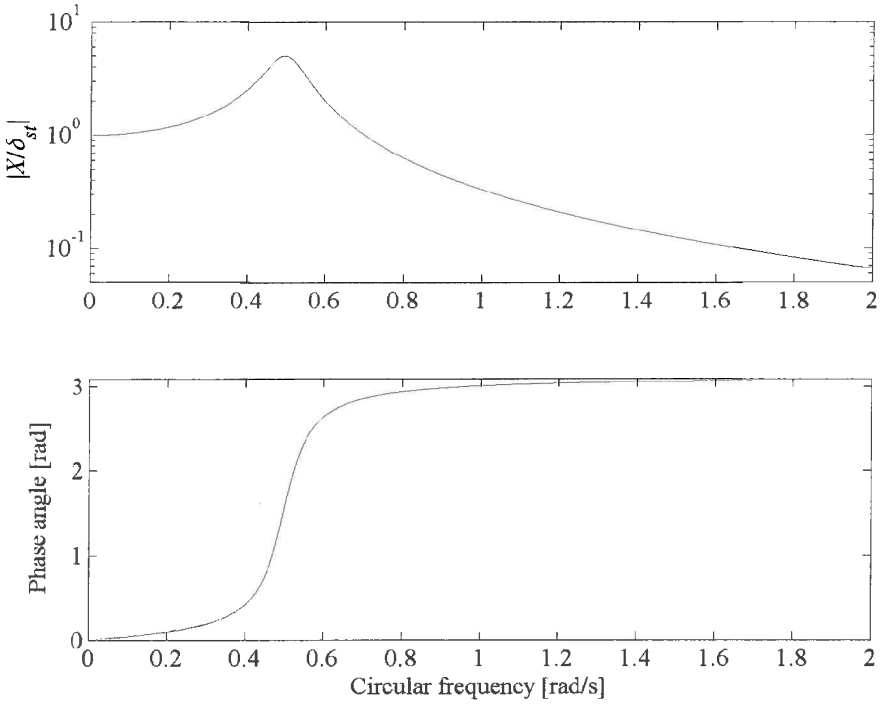

Figure A.4. A typical response of mass m_1 due to force F_1 with $\omega_a = 1$, $\omega_n = 0.5$ and $\zeta = 0.1$

The natural frequency can be seen on the FRF plot. The plot also shows the response of the system at the anti-resonant frequency (the exact point of anti-resonance might not be clear). The undamped natural frequency for this single degree-of-freedom system is given by equation A.23:

$$f_n = \frac{1}{2\pi}\sqrt{\frac{k}{m_1 + m_B\left(1-\frac{R}{r}\right)^2 + \frac{I_G}{r^2}}} \qquad \textbf{(A.23)}$$

APPENDIX B

Mathematical model of a two D.O.F. vibration absorber system

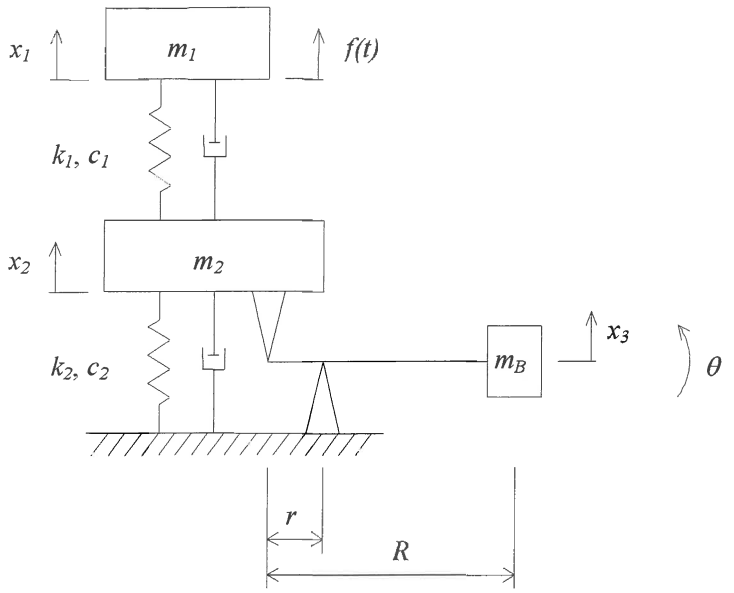

Figure B.1 A 2 degree-of-freedom vibration absorber system

The kinetic energy of the system in figure B.1 is given by equation B.1:

$$T = \frac{1}{2}\left(m_1\dot{x}_1^2 + m_2\dot{x}_2^2 + m_B\dot{x}_3^2 + I_G\dot{\theta}^2\right) \quad \textbf{(B.1)}$$

I_G is the moment of inertia of the mass m_B about its mass centre. The relation between x_3, θ, and x_2 are given by equations B.2 and B.3 (refer to figure B.2):

$$x_3 = \left(1 - \frac{R}{r}\right)x_2 \quad \textbf{(B.2)}$$

$$\theta \approx -\frac{x_2}{r} \quad \textbf{(B.3)}$$

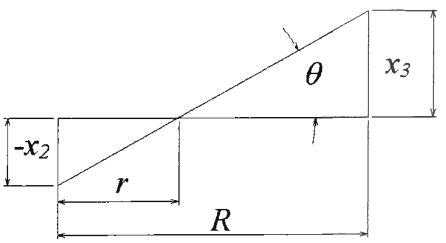

Figure B.2 Schematic of relationship between variables

Substituting these relations in equation B.1 results in the following:

$$T = \frac{1}{2}\left[m_1 \dot{x}_1^2 + \left(m_2 + \left(1 - \frac{R}{r}\right)^2 m_B + \frac{I_G}{r^2} \right) \dot{x}_2^2 \right] \tag{B.4}$$

From equation B.4 the kinetic terms in the Lagrange's equations can be derived:

$$\frac{d}{dt}\left(\frac{\partial T}{\partial \dot{x}_1}\right) = m_1 \ddot{x}_1 \tag{B.5}$$

$$\frac{d}{dt}\left(\frac{\partial T}{\partial \dot{x}_2}\right) = \left(m_2 + \left(1 - \frac{R}{r}\right)^2 m_B + \frac{I_G}{r^2} \right) \ddot{x}_2 \tag{B.6}$$

The elastic energy is given by:

$$V = \frac{1}{2}\left(k_1 (x_1 - x_2)^2 + k_2 x_2^2 \right) \tag{B.7}$$

From equation B.7 the elastic terms in the Lagrange's equations can be derived:

$$\frac{\partial V}{\partial x_1} = k_1 x_1 - k_1 x_2 \tag{B.8}$$

$$\frac{\partial V}{\partial x_2} = -k_1 x_1 + k_1 x_2 + k_2 x_2 \tag{B.9}$$

The Rayleigh function is given by:

$$R = \frac{1}{2}\left(c_1 (\dot{x}_1 - \dot{x}_2)^2 + c_2 \dot{x}_2^2 \right) \tag{B.10}$$

From equation B.10 the damping terms in the Lagrange's equations can be derived:

$$\frac{\partial R}{\partial \dot{x}_1} = c_1 \dot{x}_1 - c_1 \dot{x}_2 \tag{B.11}$$

$$\frac{\partial R}{\partial \dot{x}_2} = -c_1 \dot{x}_1 + c_1 \dot{x}_2 + c_2 \dot{x}_2 \tag{B.12}$$

The mass matrix is given by equations B.5 and B.6:

$$[M] = \begin{bmatrix} m_1 & 0 \\ 0 & m_2 + \left(1 - \frac{R}{r}\right)^2 m_B + \frac{I_G}{r^2} \end{bmatrix} \tag{B.13}$$

The stiffness matrix is given by equations B.8 and B.9:

$$[K] = \begin{bmatrix} k_1 & -k_1 \\ -k_1 & k_1 + k_2 \end{bmatrix} \tag{B.14}$$

The damping matrix is given by equations B.11 and B.12:

$$[C]=\begin{bmatrix} c_1 & -c_1 \\ -c_1 & c_1+c_2 \end{bmatrix} \tag{B.15}$$

The complete equation of motion (B.17) can be formulated by substituting the expressions in the Lagrange equation (B.16) with those found in equations B.5 and B.6, B.8 and B.9 and B.11 and B.12.

$$\begin{bmatrix} m_1 & 0 \\ 0 & m_2+\left(1-\frac{R}{r}\right)^2 m_B+\frac{I_G}{r^2} \end{bmatrix}\begin{bmatrix} \ddot{x}_1 \\ \ddot{x}_2 \end{bmatrix}+\begin{bmatrix} c_1 & -c_1 \\ -c_1 & c_1+c_2 \end{bmatrix}\begin{bmatrix} \dot{x}_1 \\ \dot{x}_2 \end{bmatrix}+\begin{bmatrix} k_1 & -k_1 \\ -k_1 & k_1+k_2 \end{bmatrix}\begin{bmatrix} x_1 \\ x_2 \end{bmatrix}=\begin{bmatrix} F_0\sin(\omega t) \\ 0 \end{bmatrix} \tag{B.16}$$

The frequency response of the system to a force vector can be found by substituting the assumed solution and its derivatives (A.12, A.13 and A.14) as well as the harmonic force (A.15) into the equation of motion (B.17). The frequency response to a force vector $F(i\omega)$ is shown in equation B.22.

$$\begin{bmatrix} X_1 \\ X_2 \end{bmatrix}=\begin{bmatrix} -\omega^2 m_1+i\omega c_1+k_1 & -i\omega c_1-k_1 \\ -i\omega c_1-k_1 & -\omega^2\left[m_2+m_B\left(1-\frac{R}{r}\right)^2+\frac{I_G}{r^2}\right]+i\omega(c_1+c_2)+k_1+k_2 \end{bmatrix}^{-1}\begin{bmatrix} F_1 \\ F_2 \end{bmatrix} \tag{B.17}$$

The response at m_2 can be found by calculating the inverse of the system matrix:

$$\frac{X_2}{F_1}=\frac{-a_{21}}{a_{11}a_{22}-a_{21}a_{12}}$$

$$=\frac{i\omega c_1+k_1}{\left(-\omega^2 m_1+i\omega c_1+k_1\right)\left(-\omega^2\left[m_2+m_B\left(1-\frac{R}{r}\right)^2+\frac{I_G}{r^2}\right]+i\omega(c_1+c_2)+k_1+k_2\right)-(i\omega c_1+k_1)^2} \tag{B.18}$$

The transmissibility will be defined in terms of forces. For this purpose the force transmitted by the spring (F_v), the damper (F_d) and the dynamic force of the absorber (F_a) must be calculated. The first two are given by equations B.19 and B.20:

$$F_v=k_2x_2 \tag{B.19}$$

$$F_d=c_2\dot{x}_2 \tag{B.20}$$

The complete derivation of equation B.21 is shown in Appendix D.

$$F_a=-\left[m_B\left(1-\frac{R}{r}\right)\frac{R}{r}-\frac{I_G}{r^2}\right]\ddot{x}_2 \tag{B.21}$$

The transmissibility is given in terms of the forces and as a function of frequency. Equations B.19 to B.21 are rewritten using equations A.12 to A.14 and added to arrive at the total force transmitted to the foundation. The force applied at mass m_1 is given by equation B.18. The transmissibility is therefore:

$$\frac{F_o}{F_i} = \frac{\left(k_2 + i\omega c_2 + \omega^2\left[m_B\left(1-\frac{R}{r}\right)\frac{R}{r} - \frac{I_G}{r^2}\right]\right)X_2}{F_1}$$

$$= \frac{(i\omega c_1 + k_1)\left(k_2 + i\omega c_2 + \omega^2\left[m_B\left(1-\frac{R}{r}\right)\frac{R}{r} - \frac{I_G}{r^2}\right]\right)}{\left(-\omega^2 m_1 + i\omega c_1 + k_1\right)\left(-\omega^2\left[m_2 + m_B\left(1-\frac{R}{r}\right)^2 + \frac{I_G}{r^2}\right] + i\omega(c_1+c_2) + k_1 + k_2\right) - (i\omega c_1 - k_1)^2} \quad \textbf{(B.22)}$$

The following transmissibility plot of equation B.27 illustrates the effect of c_2. The importance of low damping in the absorber is clearly evident.

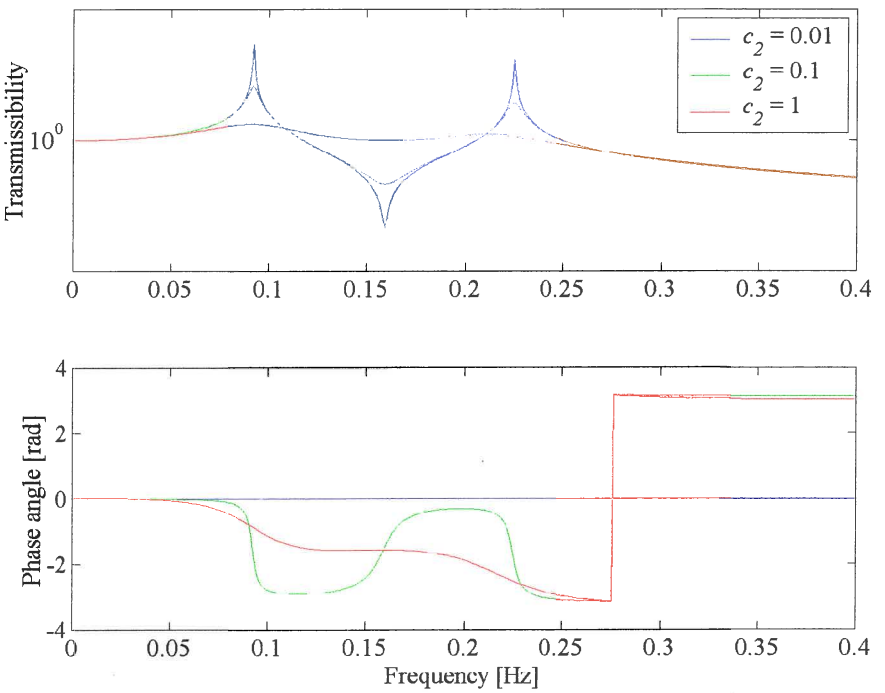

Figure B.3 A typical transmissibility plot of equation B.26 showing the effects of damping ($c_1 = 0$, $c_2 = 0.01$, $m_B = 0.5$, $m_1 = m_2 = k_1 = k_2 = 1$ and $R/r = 2$)

The aim of the absorber is to minimise the force transferred to the foundation. This will be achieved when the numerator in the transmissibility equation (B.22) is equal to zero:

$$k_2 + i\omega c_2 + \omega^2\left[m_B\left(1-\frac{R}{r}\right)\frac{R}{r}-\frac{I_G}{r^2}\right]=0 \qquad \textbf{(B.23)}$$

The non-trivial solution for the undamped isolation frequency ($c_2 = 0$) is:

$$f_a = \frac{1}{2\pi}\sqrt{\frac{-k_2}{m_B\left(1-\frac{R}{r}\right)\frac{R}{r}-\frac{I}{r^2}}} \qquad \textbf{(B.24)}$$

The response of the screen to the applied force after the addition of the absorber is of critical importance since it will influence its effective operation. The response of the screen is given by equation B.25. From this equation it is evident that the response of the screen will be influenced by the addition of an absorber. The effect must be minimised through proper choice of parameters and the applied force must be adjusted to compensate.

$$\frac{X_1}{F_1}=\frac{a_{22}}{a_{11}a_{22}-a_{21}a_{12}}$$

$$=\frac{-\omega^2\left[m_2+m_B\left(1-\frac{R}{r}\right)^2+\frac{I_G}{r^2}\right]+i\omega(c_1+c_2)+k_1+k_2}{\left(-\omega^2 m_1+i\omega c_1+k_1\right)\left(-\omega^2\left[m_2+m_B\left(1-\frac{R}{r}\right)^2+\frac{I_G}{r^2}\right]+i\omega(c_1+c_2)+k_1+k_2\right)-(i\omega c_1+k_1)^2} \qquad \textbf{(B.25)}$$

The following plot of equation B.25 illustrates the forced response of the system at mass m_1.

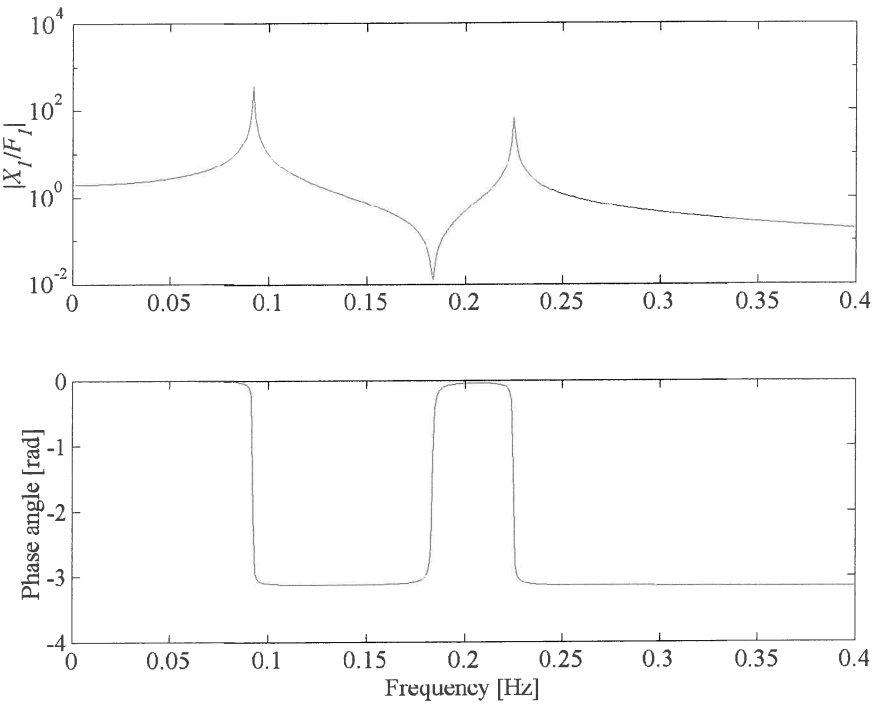

Figure B.4 A typical response of mass m_1 due to force F_1 (α_{11})
($c_1 = 0$, $c_2 = 0.01$, $m_B = 0.5$, $m_1 = m_2 = k_1 = k_2 = 1$ and $R/r = 2$)

The natural frequencies can be seen on both figure B.4 and B.5. The figures also show the response of the system at the isolation frequency (the exact point of isolation might not be clear). The natural frequencies cannot easily be found analytically but are rather calculated numerically with an eigenvalue approach.

The following plot of equation B.18 illustrates the forced response of the system at mass m_2. The 2 degree-of-freedom model can be used to model a screen mounted on an absorber.

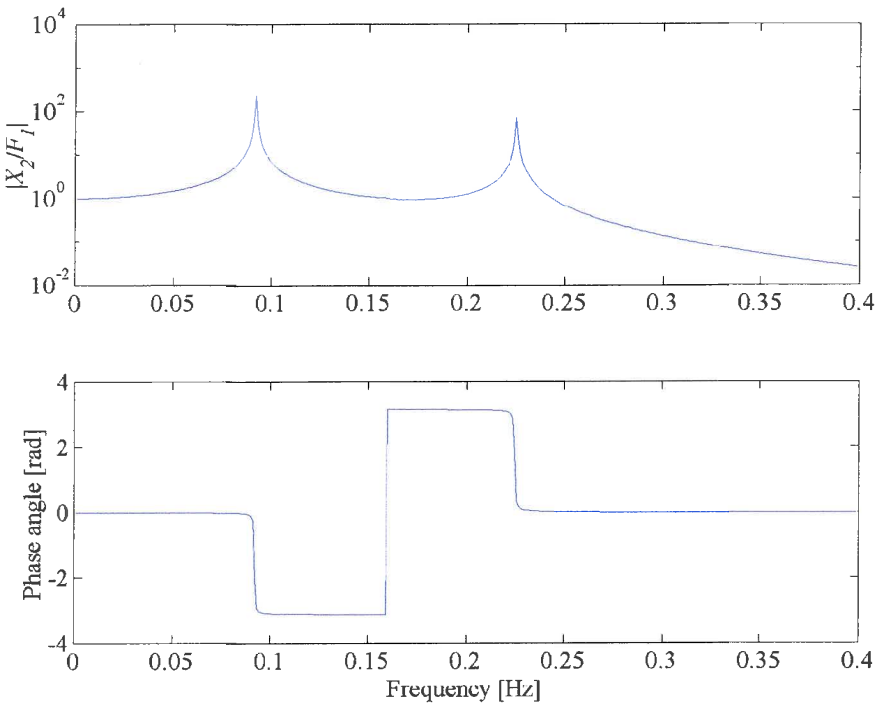

Figure B.5 A typical response of mass m_2 due to force F_1 (α_{21}) with $c_1 = 0$, $c_2 = 0.01$, $m_B = 0.5$, $m_1 = m_2 = k_1 = k_2 = 1$ and $R/r = 2$

APPENDIX C

Mathematical model of a 3 D.O.F. vibration absorber system

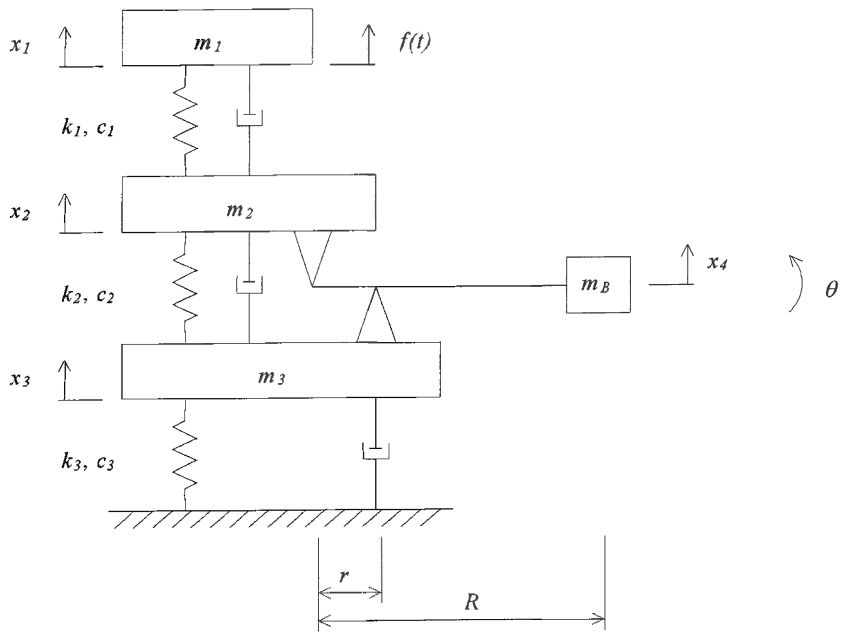

Figure C.1 A three degree-of-freedom system including a vibration absorber

The kinetic energy of the system in figure C.1 is given by equation C.1:

$$T = \frac{1}{2}\left(m_1\dot{x}_1^2 + m_2\dot{x}_2^2 + m_3\dot{x}_3^2 + m_B\dot{x}_4^2 + I_G\dot{\theta}^2\right) \qquad \textbf{(C.1)}$$

I_G is the moment of inertia of the mass m_B about its mass centre. The relation between x_4, θ, x_3 and x_2 are given by equations C.2 and C.3 (refer to figure C.2):

$$x_4 = \left(1 - \frac{R}{r}\right)x_2 + \frac{R}{r}x_3 \qquad \textbf{(C.2)}$$

$$\theta \approx \frac{x_3 - x_2}{r} \qquad \textbf{(C.3)}$$

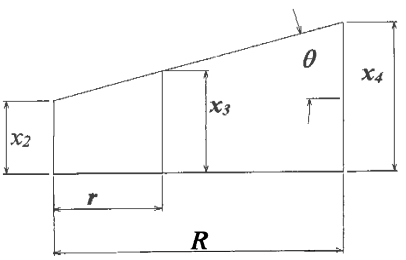

Figure C.2. Schematic of relationship between variables

Substituting these relations in equation C.1 results in the following:

$$T=\frac{1}{2}\left[m_1\dot{x}_1^2+\left(m_2+\left(1-\frac{R}{r}\right)^2 m_B+\frac{I_G}{r^2}\right)\dot{x}_2^2+\left(m_3+\left(\frac{R}{r}\right)^2 m_B+\frac{I_G}{r^2}\right)\dot{x}_3^2+\left(2\left(1-\frac{R}{r}\right)\left(\frac{R}{r}\right)m_B-2\frac{I_G}{r^2}\right)\dot{x}_2\dot{x}_3\right] \tag{C.4}$$

From equation C.4 the kinetic terms in the Lagrange's equations can be derived:

$$\frac{d}{dt}\left(\frac{\partial T}{\partial \dot{x}_1}\right)=m_1\ddot{x}_1 \tag{C.5}$$

$$\frac{d}{dt}\left(\frac{\partial T}{\partial \dot{x}_2}\right)=\left(m_2+\left(1-\frac{R}{r}\right)^2 m_B+\frac{I_G}{r^2}\right)\ddot{x}_2+\left(\left(1-\frac{R}{r}\right)\frac{R}{r}m_B-\frac{I_G}{r^2}\right)\ddot{x}_3 \tag{C.6}$$

$$\frac{d}{dt}\left(\frac{\partial T}{\partial \dot{x}_3}\right)=\left(m_3+\left(\frac{R}{r}\right)^2 m_B+\frac{I_G}{r^2}\right)\ddot{x}_3+\left(\left(1-\frac{R}{r}\right)\frac{R}{r}m_B-\frac{I_G}{r^2}\right)\ddot{x}_2 \tag{C.7}$$

The elastic energy is given by:

$$V=\frac{1}{2}\left(k_1(x_1-x_2)^2+k_2(x_2-x_3)^2+k_3x_3^2\right) \tag{C.8}$$

From equation C.8 the elastic terms in the Lagrange's equations can be derived:

$$\frac{\partial V}{\partial x_1}=k_1x_1-k_1x_2 \tag{C.9}$$

$$\frac{\partial V}{\partial x_2}=-k_1x_1+k_1x_2+k_2x_2-k_2x_3 \tag{C.10}$$

$$\frac{\partial V}{\partial x_3}=-k_2x_2+k_2x_3+k_3x_3 \tag{C.11}$$

The Rayleigh function is given by:

$$R=\frac{1}{2}\left(c_1(\dot{x}_1-\dot{x}_2)^2+c_2(\dot{x}_2-\dot{x}_3)^2+c_3\dot{x}_3^2\right) \tag{C.12}$$

From equation C.12 the damping terms in the Lagrange's equations can be derived:

$$\frac{\partial R}{\partial \dot{x}_1}=c_1\dot{x}_1-c_1\dot{x}_2 \tag{C.13}$$

$$\frac{\partial R}{\partial \dot{x}_2}=-c_1\dot{x}_1+c_1\dot{x}_2+c_2\dot{x}_2-c_2\dot{x}_3 \tag{C.14}$$

$$\frac{\partial R}{\partial \dot{x}_3}=-c_2\dot{x}_2+c_2\dot{x}_3+c_3\dot{x}_3 \tag{C.15}$$

The mass matrix is given by equations C.5, C.6 and C.7:

$$[M]=\begin{bmatrix} m_1 & 0 & 0 \\ 0 & m_2+\left(1-\frac{R}{r}\right)^2 m_B+\frac{I_G}{r^2} & \left(1-\frac{R}{r}\right)\frac{R}{r}m_B-\frac{I_G}{r^2} \\ 0 & \left(1-\frac{R}{r}\right)\frac{R}{r}m_B-\frac{I_G}{r^2} & m_3+\left(\frac{R}{r}\right)^2 m_B+\frac{I_G}{r^2} \end{bmatrix} \quad \textbf{(C.16)}$$

The stiffness matrix is given by equations C.9, C.10 and C.11:

$$[K]=\begin{bmatrix} k_1 & -k_1 & 0 \\ -k_1 & k_1+k_2 & -k_2 \\ 0 & -k_2 & k_2+k_3 \end{bmatrix} \quad \textbf{(C.17)}$$

The damping matrix is given by equations C.13, C.14 and C.15:

$$[C]=\begin{bmatrix} c_1 & -c_1 & 0 \\ -c_1 & c_1+c_2 & -c_2 \\ 0 & -c_2 & c_2+c_3 \end{bmatrix} \quad \textbf{(C.18)}$$

The complete equation of motion (C.20) can be formulated by substituting the expressions in the Lagrange's equations (A.10) with those found in equations C.5 to C.7, C.9 to C.11 and C.13 to C.15:

$$[M]\{\ddot{x}\}+[C]\{\dot{x}\}+[K]\{x\}=\{f\} \quad \textbf{(C.20)}$$

The frequency response of the system to a force vector can be found by substituting the assumed solution and its derivatives (A.12, A.13 and A.14) as well as the harmonic force (A.15) into the equation of motion (C.20). The frequency response to a force vector $F(i\omega)$ is shown in equation C.25.

The transmissibility is calculated numerically from equations C.21 and C.22

$$\begin{Bmatrix} X_1 \\ X_2 \\ X_3 \end{Bmatrix} = \left[-\omega^2[M]+i\omega[C]+[K]\right]^{-1}\begin{Bmatrix} F_1 \\ F_2 \\ F_3 \end{Bmatrix} \quad \textbf{(C.21)}$$

$$T_{ij}=\left|\frac{X_i}{X_j}\right| \quad \textbf{(C.22)}$$

The following transmissibility plot (T_{31}) described by equation C.22 illustrates the effect of c_2. The importance of low damping in the absorber is clearly evident. It is not always possible to see all the natural frequencies on the transmissibility plot. The position of the natural frequency is however extremely important and will be discussed later in this appendix.

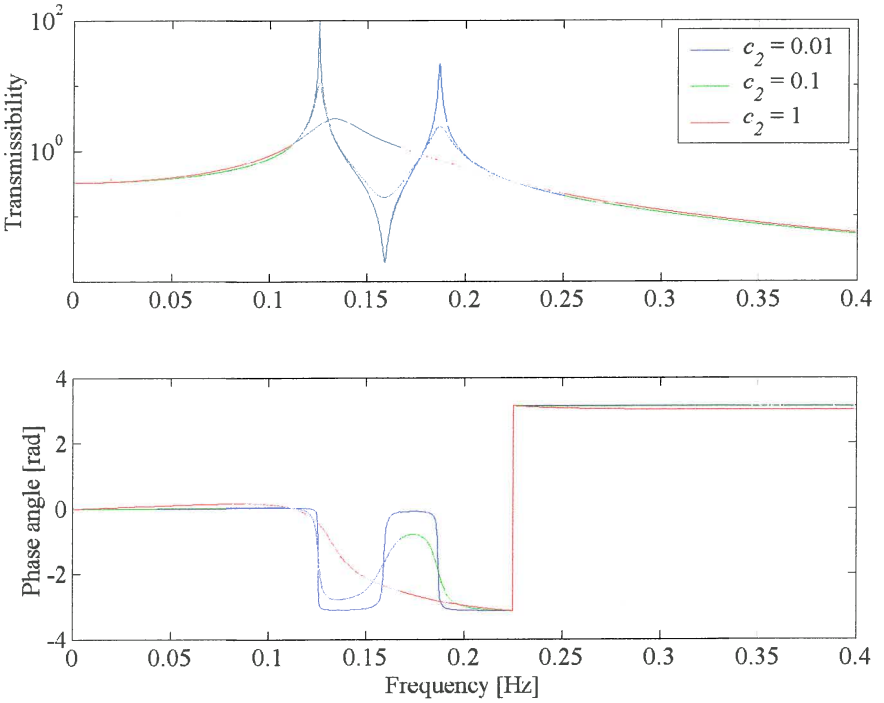

Figure C.3 A typical transmissibility plot of equation C.22 (T_{31}) showing the effects of damping ($c_1 = c_3 = 0$, $m_B = 0.5$, $m_3 = k_3 = k_2 = 1$, $I_G = 0$ and $R/r = 2$)

In order to be able to formulate an expression for the isolation frequency, an analytical expression will be found for the transmissibility between mass m_2 and mass m_3. Equation C.23 was found by substituting the assumed solution and its derivatives (A.12, A.13 and A.14) in the 3rd equation of the set of equations described by equation C.20.

$$\frac{X_3}{X_2} = \frac{k_2 + i\omega c_2 + \omega^2\left(m_B\left(1-\frac{R}{r}\right)\frac{R}{r} - \frac{I_G}{r^2}\right)}{k_2 + k_3 + i\omega(c_2 + c_3) - \omega^2\left(m_3 + m_B\left(\frac{R}{r}\right)^2 + \frac{I_G}{r^2}\right)} \qquad \textbf{(C.23)}$$

The aim of the absorber is to minimise the force transferred to the foundation by minimising the motion of mass m_3. This will be achieved when the numerator in the transmissibility equation (C.23) is equal to zero:

$$k_2 + i\omega c_2 + \omega^2\left(m_B\left(1-\frac{R}{r}\right)\frac{R}{r} - \frac{I_G}{r^2}\right) = 0 \qquad \textbf{(C.24)}$$

The non-trivial solution for the undamped isolation frequency ($c_2 = 0$) is:

$$f_a = \frac{1}{2\pi}\sqrt{\frac{-k_2}{m_B\left(1-\frac{R}{r}\right)\frac{R}{r} - \frac{I_G}{r^2}}} \qquad \textbf{(C.25)}$$

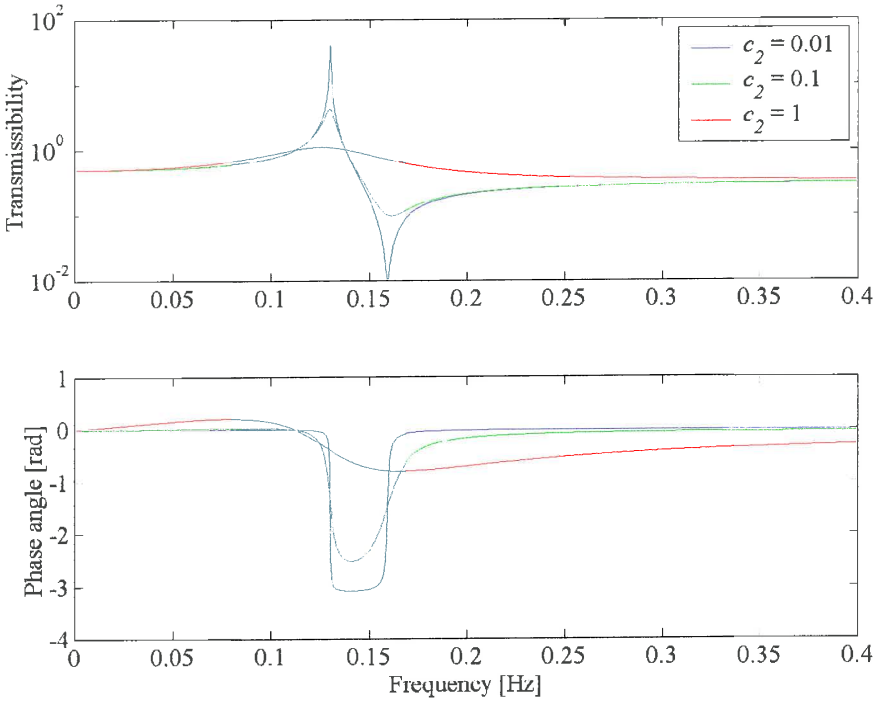

Figure C.4 A typical transmissibility plot of equation C.23 (T_{32}) showing the effects of damping ($c_1 = c_3 = 0$, $m_B = 0.5$, $m_3 = k_3 = k_2 = 1$, $I_G = 0$ and $R/r = 2$)

The response of the screen to the applied force after the addition of the absorber is of critical importance since it will influence its effective operation. The response of the screen is given by equation C.21. From this equation it is evident that the response of the screen will be influenced by the addition of an absorber. The effect must be minimised through proper choice of parameters and the applied force must be adjusted to compensate.

The following figures show the response at mass m_1 and m_3 due to a force acting on mass m_1. The three natural frequencies are clearly visible. The figures also show the response of the system at the anti-resonant frequency. Figure C.6 shows that mass m_3 has low response at anti-resonance.

The 3 DOF model can be used to model a screen mounted on an absorber when the stiffness of the support must be taken into account.

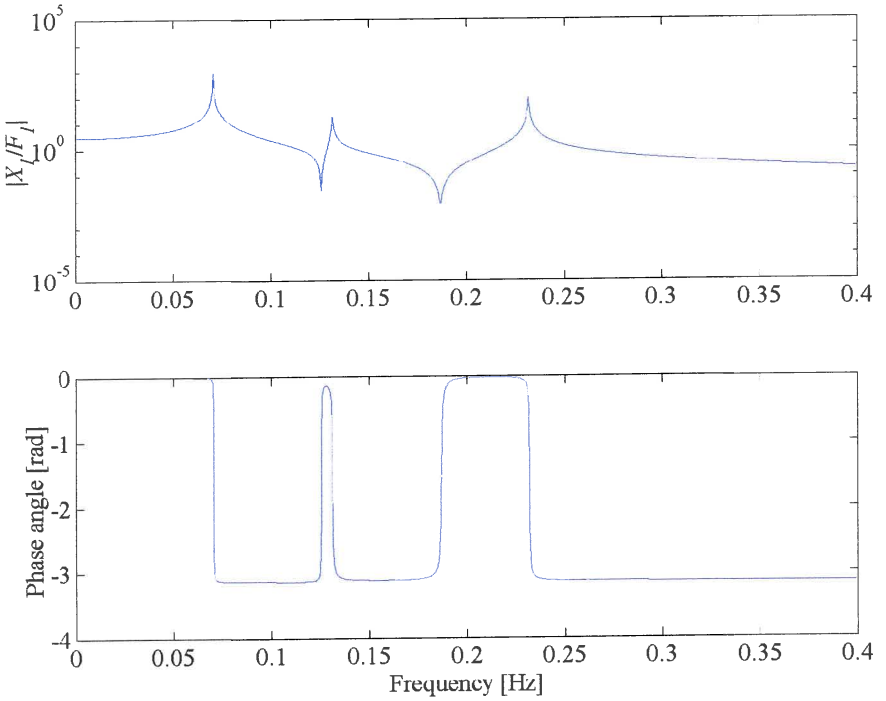

Figure C.5 The response of mass m_1 due to force F_1 (α_{11})
($c_1 = c_3 = 0$, $c_2 = 0.01$, $m_B = 0.5$, $m_1 = m_2 = m_3 = k_1 = k_2 = k_3 = 1$, $I_G = 0$ and $R/r = 2$)

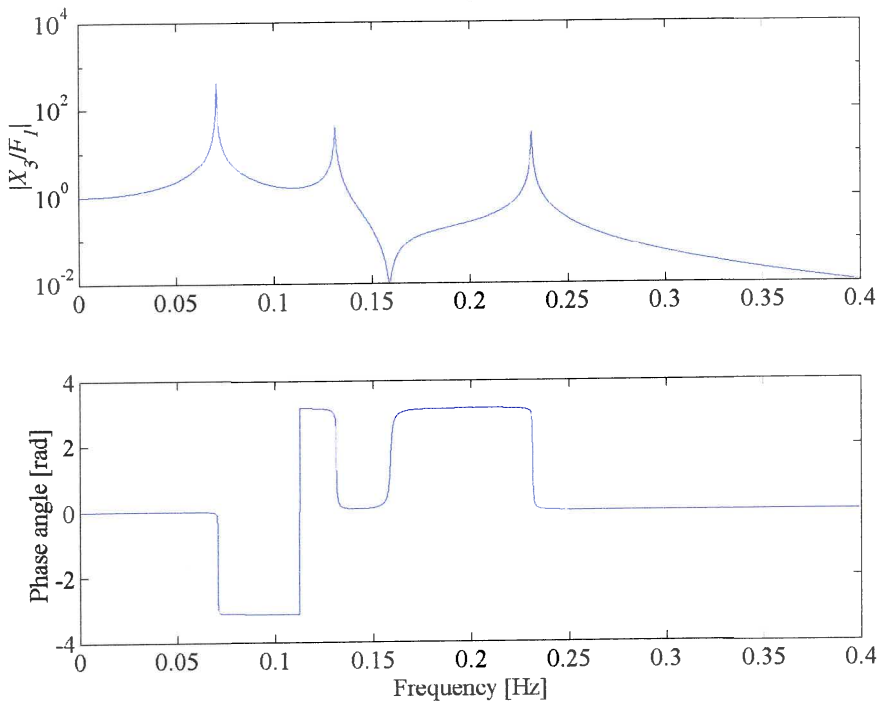

Figure C.6 The response of mass m_3 due to force F_1 (α_{31})
($c_1 = c_3 = 0$, $c_2 = 0.01$, $m_B = 0.5$, $m_1 = m_2 = m_3 = k_1 = k_2 = k_3 = 1$, $I_G = 0$ and $R/r = 2$)

APPENDIX D

Analysis of the inertial absorber force

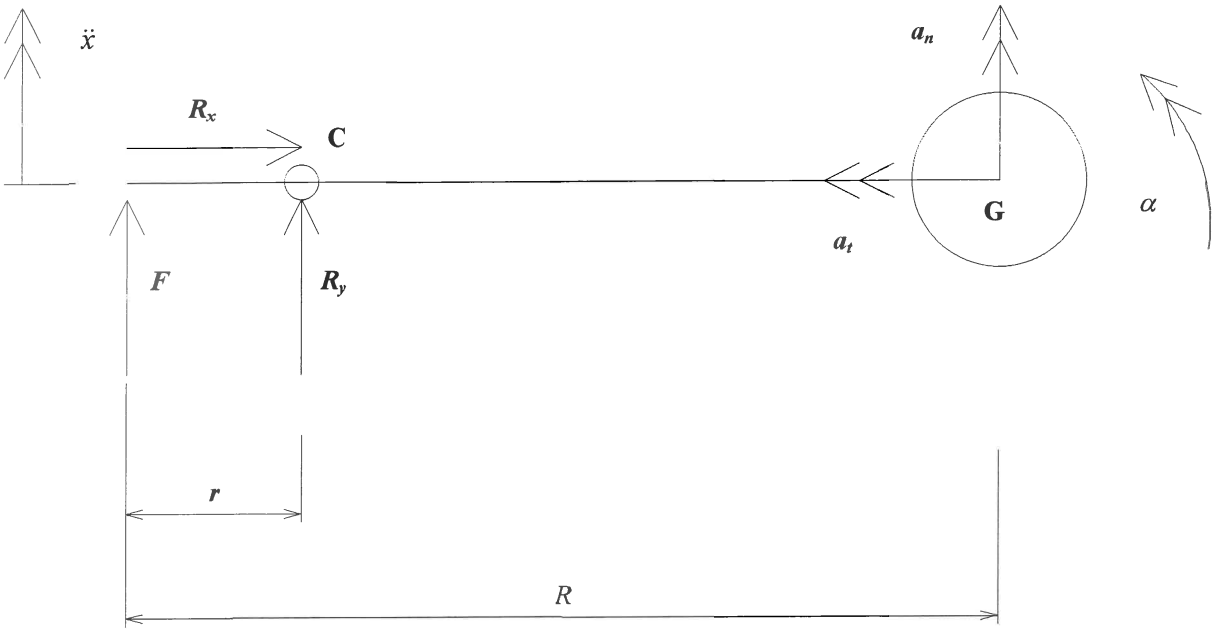

Figure D.2 Schematic of absorber pendulum

The sum of the moments about fixed pivot C is given by:

$$\begin{aligned}\Sigma M_C &= I_C\alpha \\ &= -Fr\end{aligned} \tag{D.1}$$

The sum of the forces in the x and y directions are:

$$\begin{aligned}\Sigma F_x &= -m_B a_t \\ R_x &= -m_B(R-r)\omega^2\end{aligned} \tag{D.2}$$

$$\begin{aligned}\Sigma F_y &= m_B a_n \\ F + R_y &= m_B(R-r)\alpha\end{aligned} \tag{D.3}$$

The trigonometric relationship between the linear and angular acceleration is given by:

$$\ddot{x} \approx -r\alpha \tag{D.4}$$

By substituting equation D.1 in equation D.3 the force R_y can be found as a function of the angular acceleration:

$$R_y = m_B(R-r)\alpha + \frac{I_C}{r}\alpha \tag{D.5}$$

The angular acceleration can now be substituted with the relationship given by equation D.4:

$$R_y = -\frac{m_B}{r}(R-r)\ddot{x} - \frac{I_C}{r^2}\ddot{x} \tag{D.6}$$

The following expression can be written for the moment of inertia about C using Steiner's theorem:

$$I_C = m_B(R-r)^2 + I_G \tag{D.7}$$

Substituting this relationship into equation D.6 results in:

$$\begin{aligned} R_y &= \left[-\frac{m_B}{r}(R-r) - \frac{m_B}{r^2}(R-r)^2 - \frac{I_G}{r^2} \right] \ddot{x} \\ &= \left[m_B\left(1-\frac{R}{r}\right)\frac{R}{r} - \frac{I_G}{r^2} \right] \ddot{x} \end{aligned} \tag{D.8}$$

APPENDIX E

Computational fluid dynamics analysis

E.1. Introduction

Viscous damping is a damping force that is proportional to the velocity of the fluid. To find the force it is necessary to solve the shear force on the port wall and the pressure drop across the port. Analytical equations that describe both these quantities were discussed in chapter 2, but they exist only for simple geometries. To find the total force acting on the port used in the final design computational fluid dynamics had to be used. The objective was to compare the final design with the theoretical model in order to show that a smooth inlet will reduce the amount of damping. The force found from the analytical equations was compared to CFD results for the theoretical case. This gave confidence in the method. The force acting on the port used in the final design was solved using CFD and compared to the theoretical case. This was a qualitative study and showed a marked improvement in the damping when a smooth inlet/outlet geometry was used.

E.2. Method and Model parameters

Computational fluid dynamics produce a prediction of how fluid will flow for a given situation (Shaw, 1992). To do this the numerical solutions to the equations that govern the flow must be solved. These equations can be found from the knowledge that mass and momentum must be conserved. The package used to solve the flow was STAR-CD. This package uses the finite volume method to solve the equations for the fluid flow, which is described in detail by Patankar (1980). Turbulence was included in the model using the k-ε turbulence model. This method calculates the kinetic energy k and the distribution of the dissipation rate of k denoted by ε.

The inputs needed by the CFD package are:

- the geometry of the flow domain including the computational mesh
- fluid properties
- boundary conditions
- solution control parameters

Due to its simplicity, the geometry for the theoretical model was created in STAR-CD. The geometry for the design was imported from CAD. A mesh of hexahedral cells was created. Only $1/8^{th}$ of the port was modeled to reduce the solution time. The fluid properties were the same for both models.

Table E.2 Fluid properties

Property	Value
Density [kg/m^3]	1000
Absolute viscosity	1×10^{-3}

The boundary condition was treated as a constant axial velocity inlet at the bottom and a constant axial velocity outlet at the top. It was assumed that the fluid flow would have the same velocity as the port that is forcing it. The port is moving relative to the sleeve and it is therefore possible to specify the boundary condition on the sleeve and keep the port fixed.

The velocity of the port is equal to the inlet velocity and is related to the amplitude and circular frequency by:

$$\dot{x}(t) = i\omega X e^{i\omega t}$$

By solving the damping for different inlet velocities, a lookup table can be constructed. For a fixed amplitude the damping coefficient is only a function of frequency.

The SIMPLE algorithm was used for the solution. The solution converged in 3000 iterations. The y^+ values were checked and fell within the acceptable range of 30 to 100.

The following two paragraphs will give detailed results for the two models. Graphical output of the CFD program is also included to give physical insight in the processes that cause damping.

E.3. Theoretical model

Figures E.1 to E.3 show the grid of hexahedral cells. A constant axial velocity outlet boundary condition was specified at the top and a constant axial velocity inlet at the bottom. The walls had a no-slip boundary condition. A symmetry plane was defined to reduce the size of the model. No flow is allowed perpendicular to this plane.

The port inlet and outlet are sudden contractions and expansions, which will create the maximum flow losses for this port and reservoir diameter.

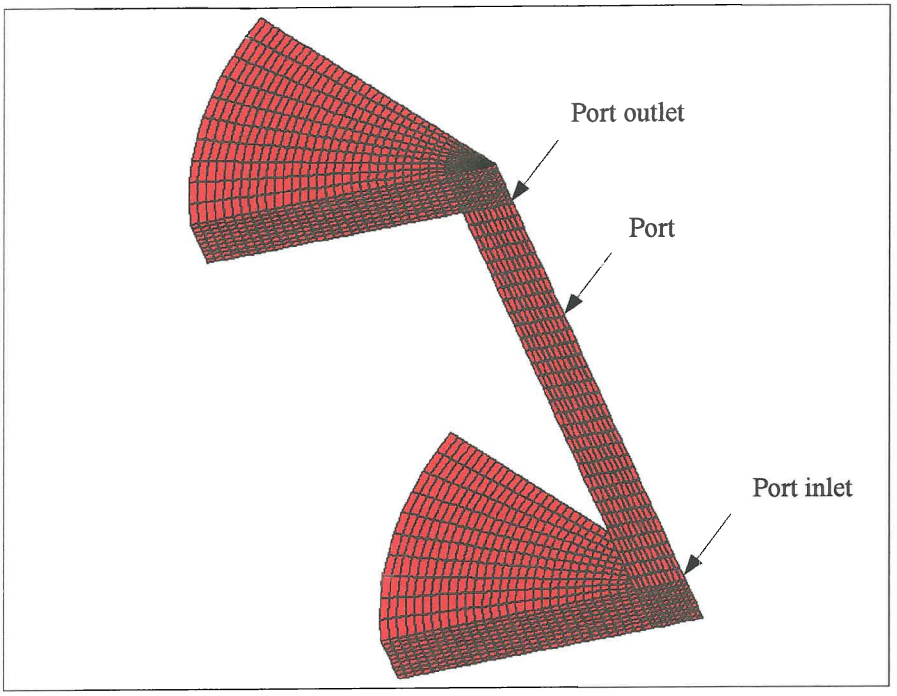

Figure E.1 3D grid for 1/8th of the flow region

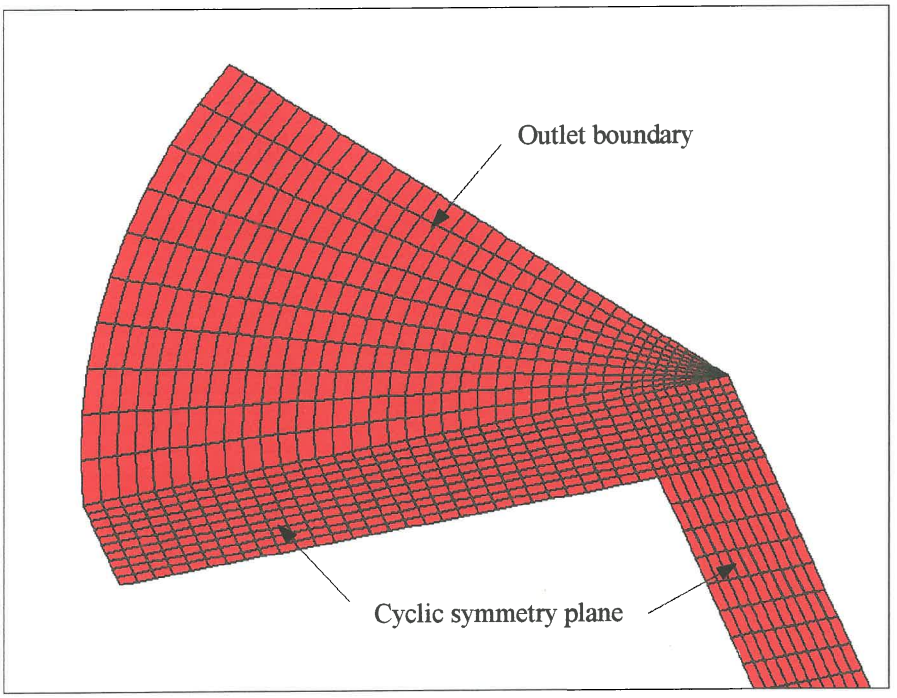

Figure E.2 Grid at the outlet

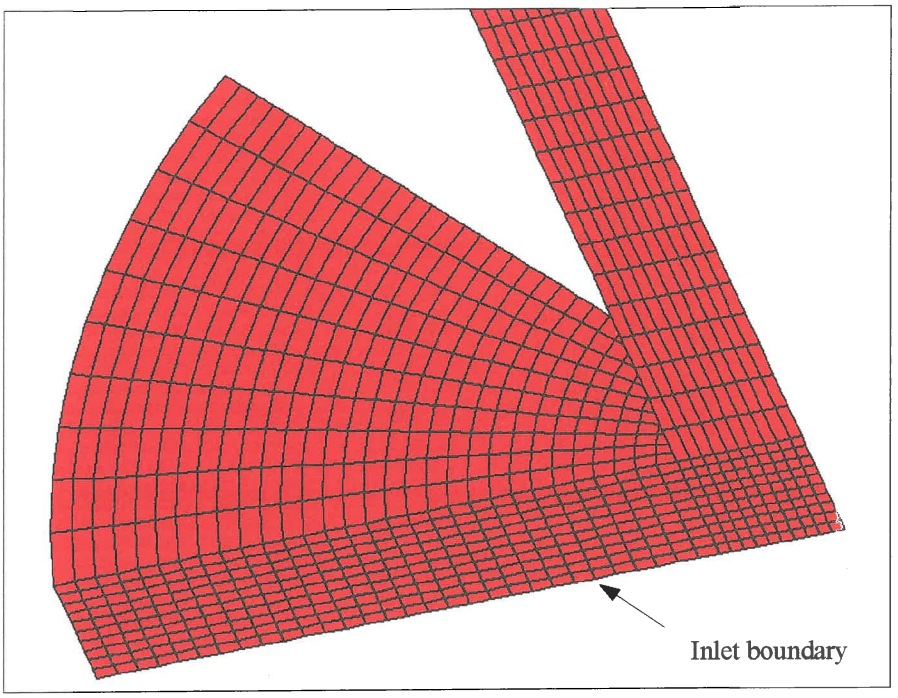

Figure E.3 Grid at the inlet

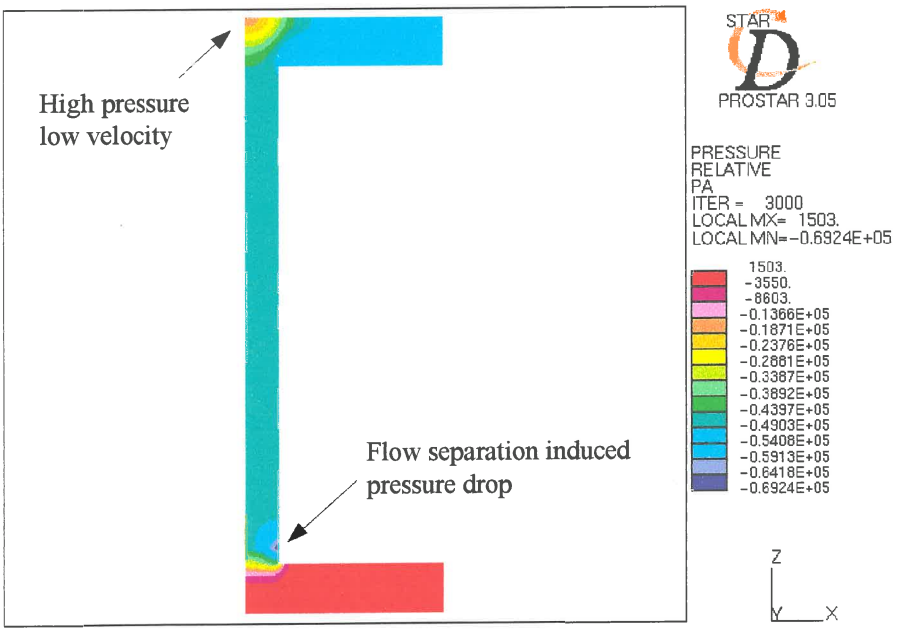

E.4 Relative pressure

On figure E.4 it can be seen that the flow separation at the inlet cause a pressure drop at the wall. The flow separation reduces the effective flow area, which accelerates the fluid. This condition can be seen in figure E.5 and E.7.

The wall had a no-slip boundary condition the effect of which can be seen in figure E.5.

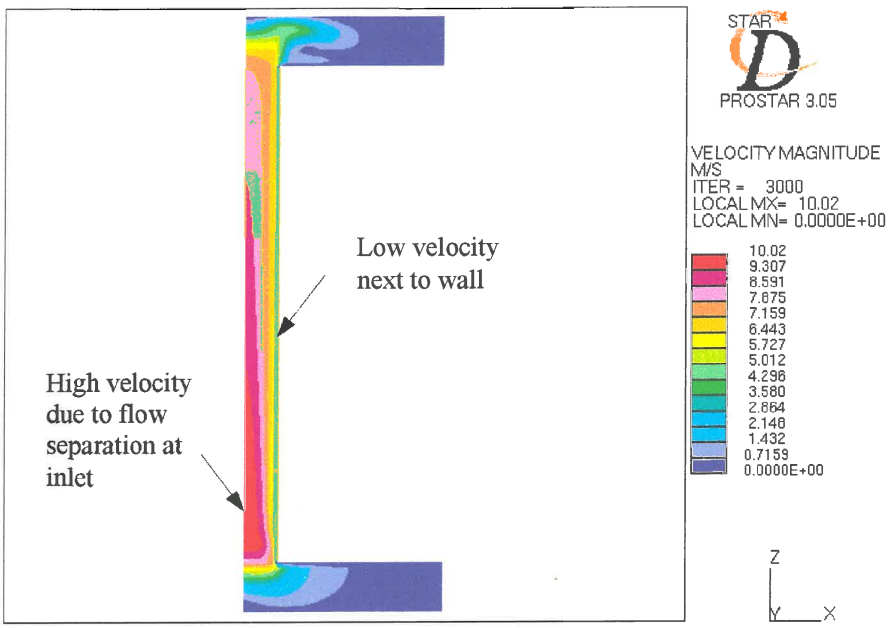

E.5 Velocity magnitude

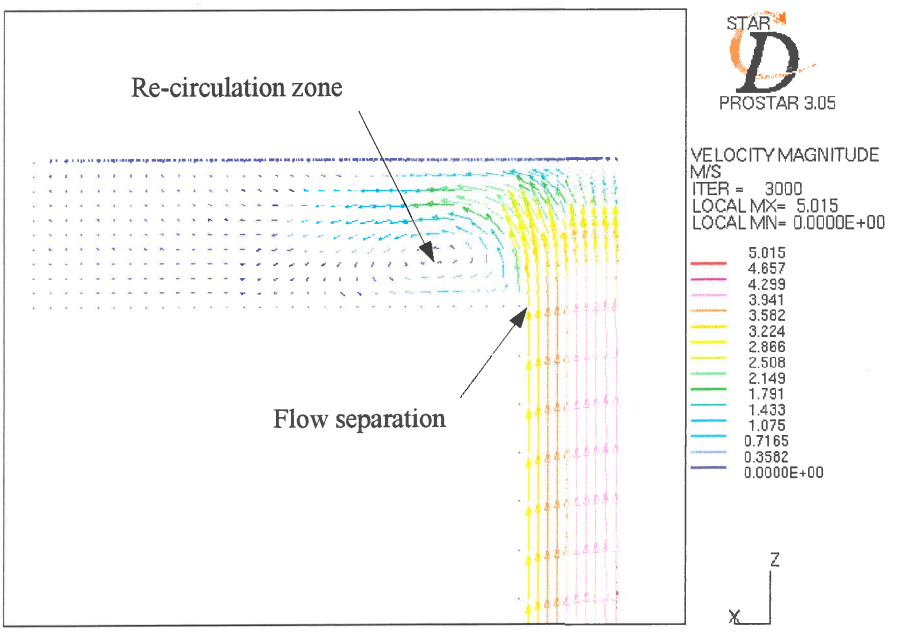

E.6 Velocity vectors at the outlet

Re-circulation at the outlet is caused by flow separation as can be seen in figure E.6. This condition will increase the damping.

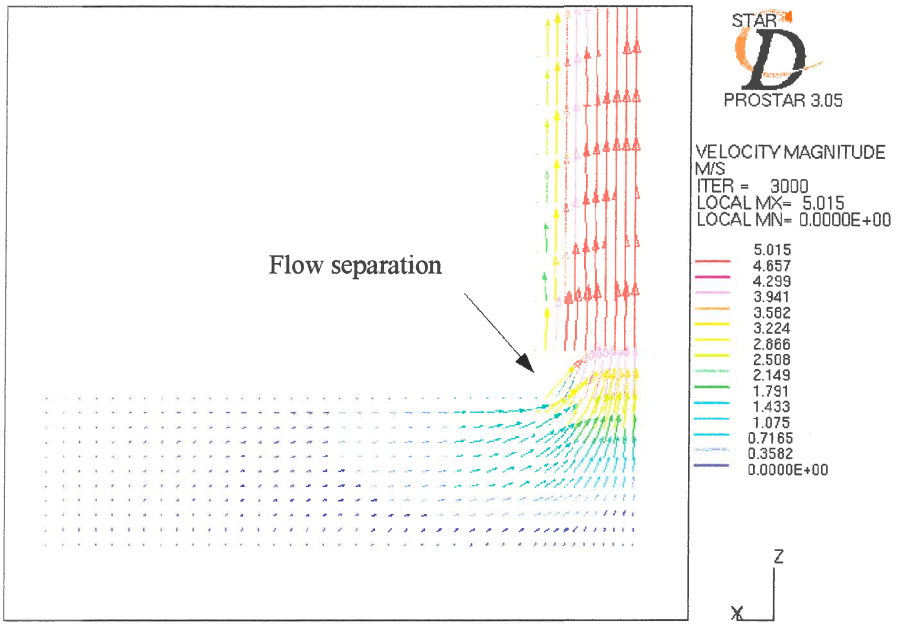

E.7 Velocity vectors at the inlet

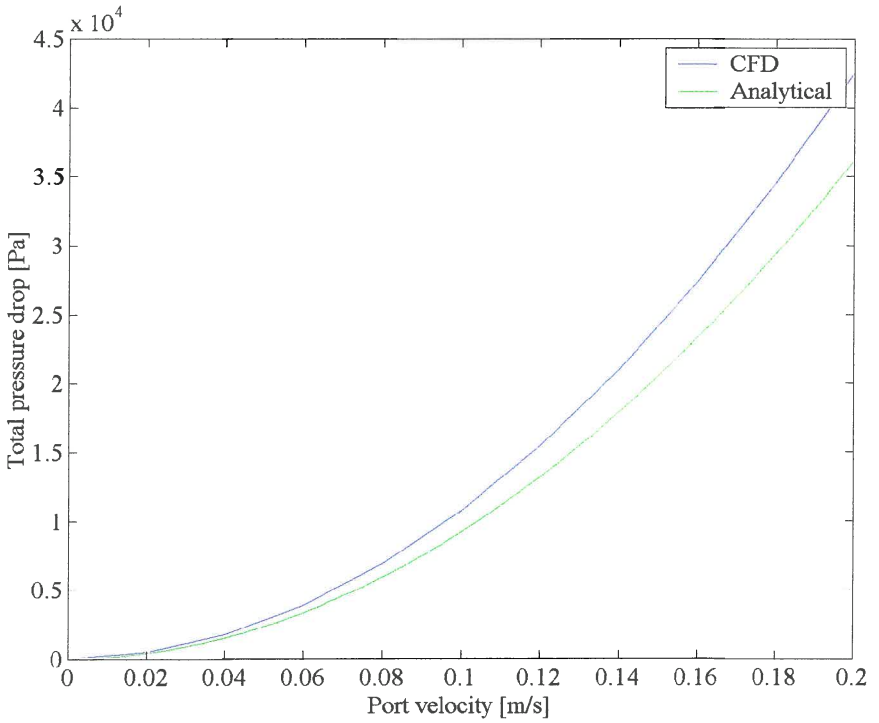

Figure E.8 Total pressure drop (Δp_T) as a function of port velocity ($\dot{x}$)

The total pressure drop is shown in figure E.8. The pressure drop at the outlet is shown in figure E.10 and is clearly much more that predicted analytically. The reason for this is the proximity of the boundary.

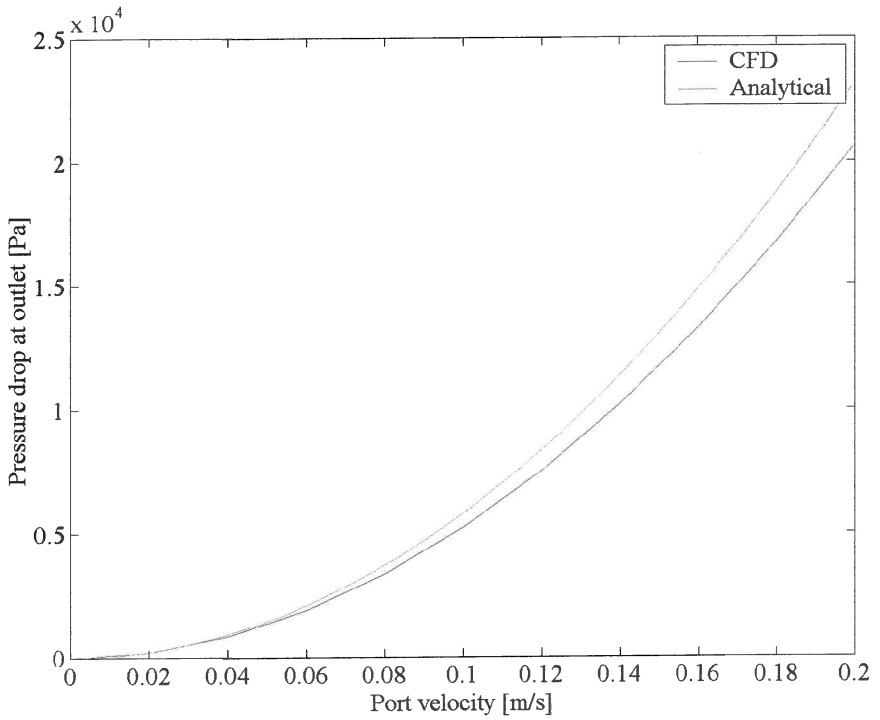

Figure E.9 The pressure drop at the outlet (Δp_o) as a function of port velocity ($\dot{x}$)

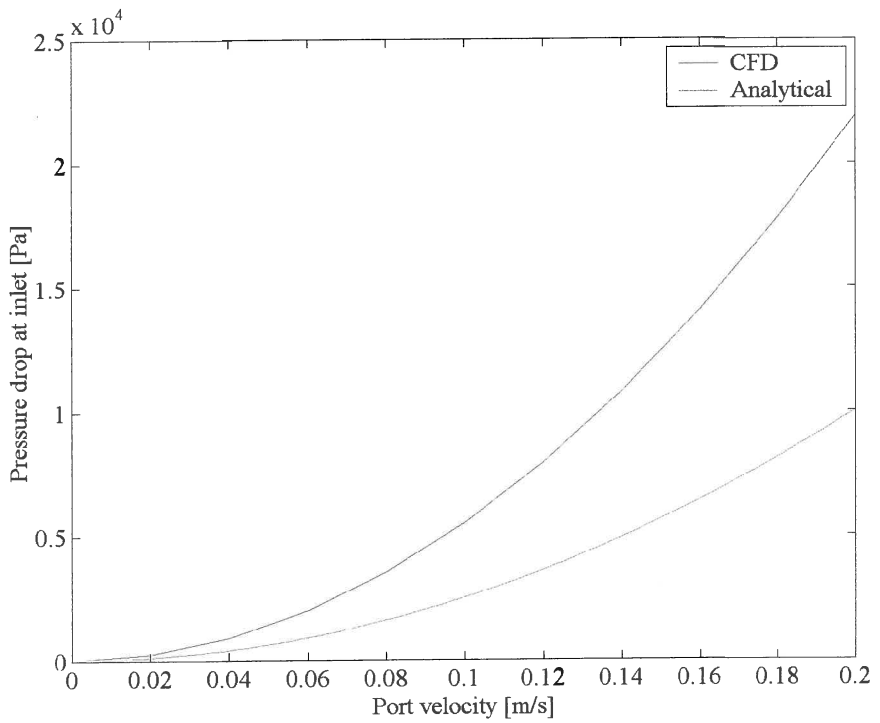

Figure E.10 The pressure drop at the inlet (Δp_i) as a function of port velocity ($\dot{x}$)

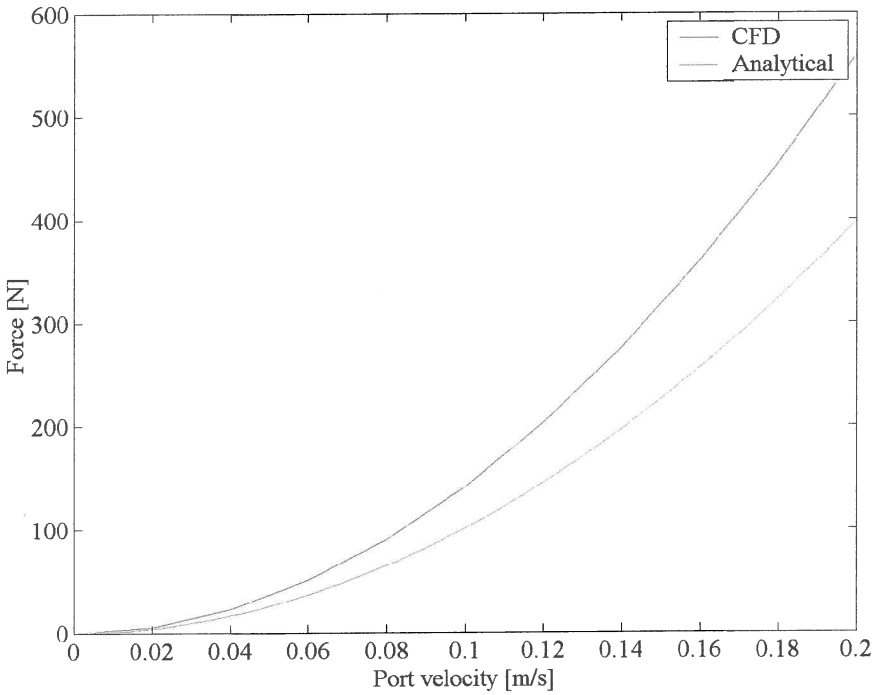

Figure E.11 Force in the z-direction (F_z) as a function of port velocity ($\dot{x}$)

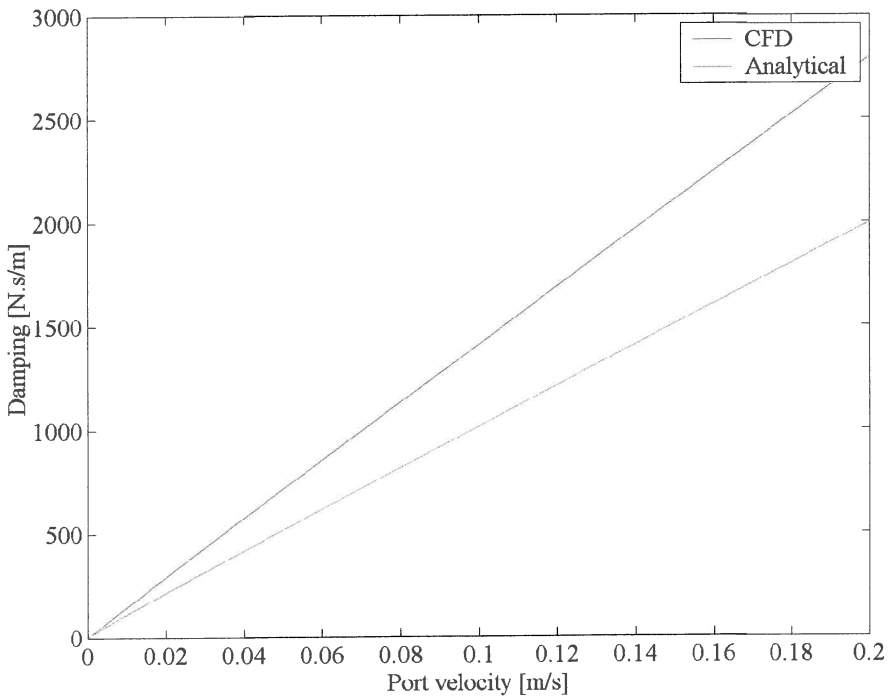

Figure E.12 Damping (c) as a function of port velocity ($\dot{x}$)

The pressure varies quadratically as can be expected from its relation with velocity (figure E.13) while the damping coefficient varies linearly as can be seen in figure E.12.

E.4. Design

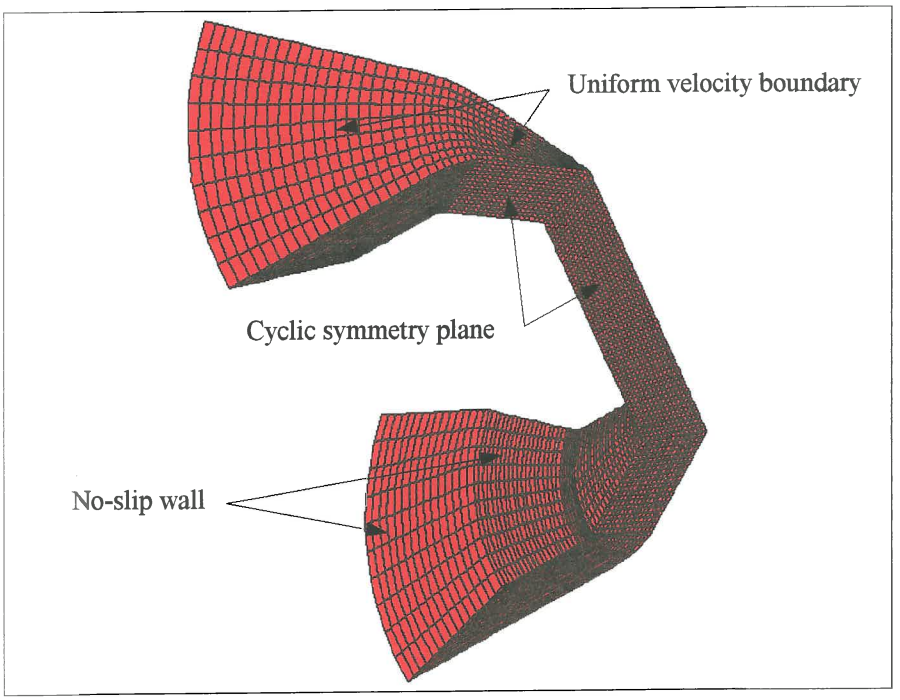

Figure E.13 3D grid for 1/8th of the flow region

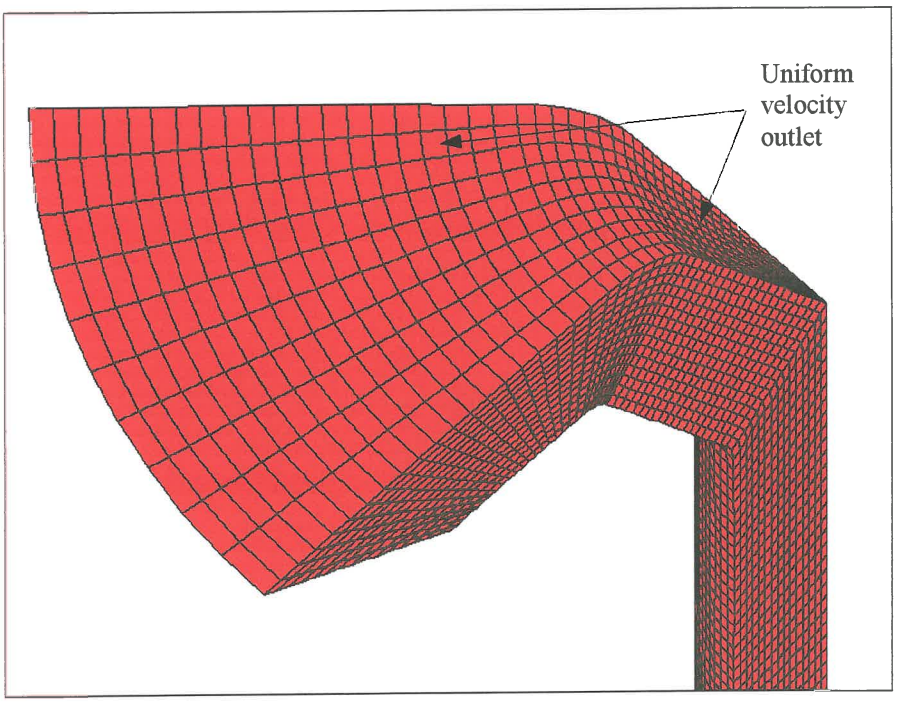

Figure E.14 Grid at the outlet

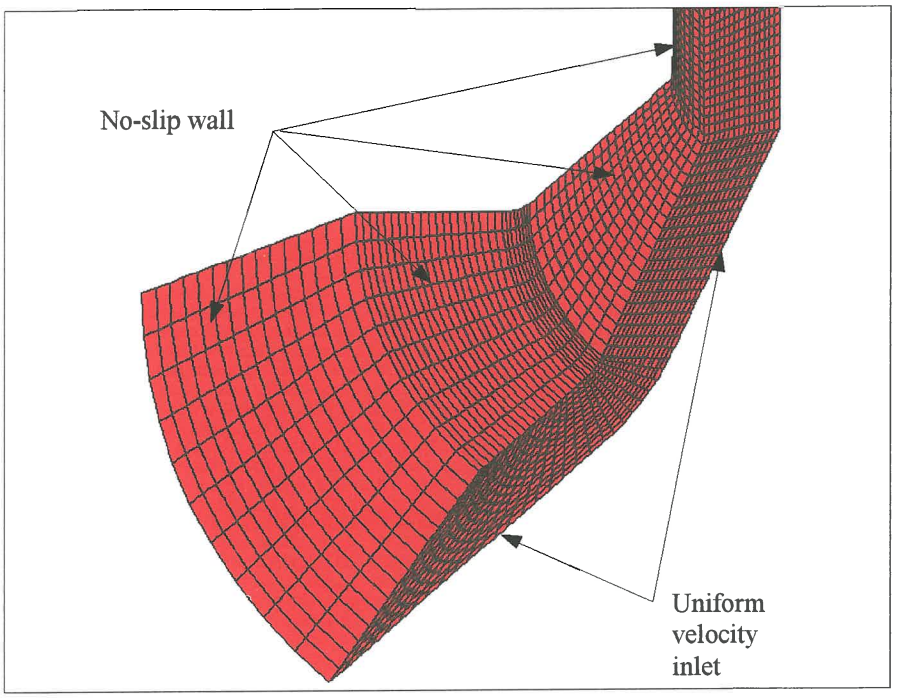

Figure E.15 Grid at the inlet

The mesh used for the final design is shown in figures E.13 to E.15. The boundary condition was a constant velocity in the z-direction on the ends of the grid. Figure E.16 show that the gradual change in area causes less flow disturbance.

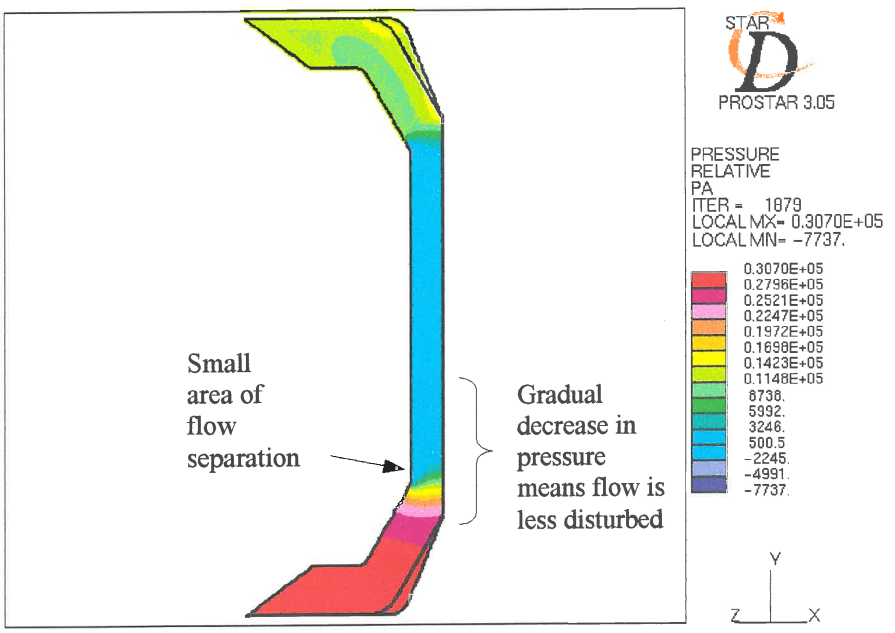

Figure E.16 Relative pressure

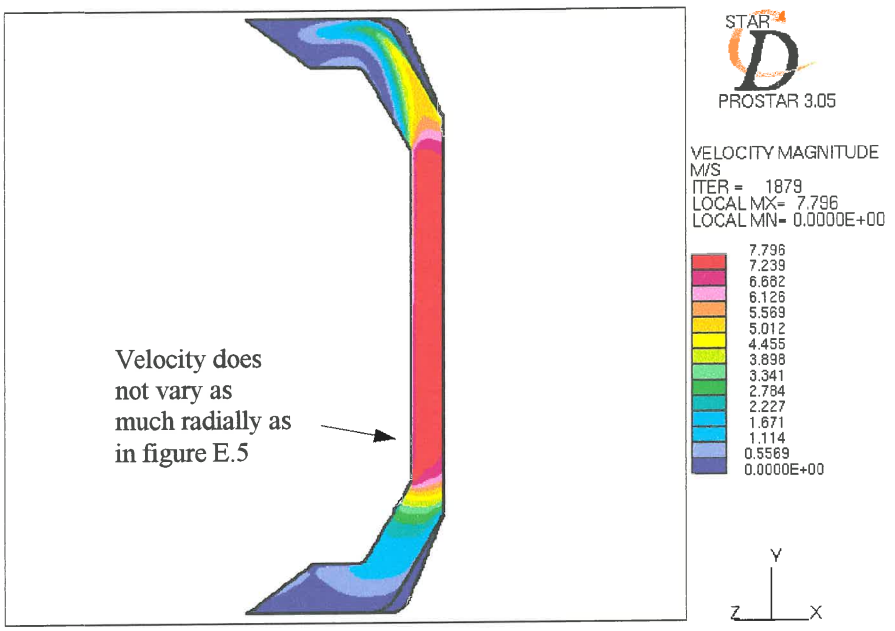

Figure E.17 Velocity magnitude

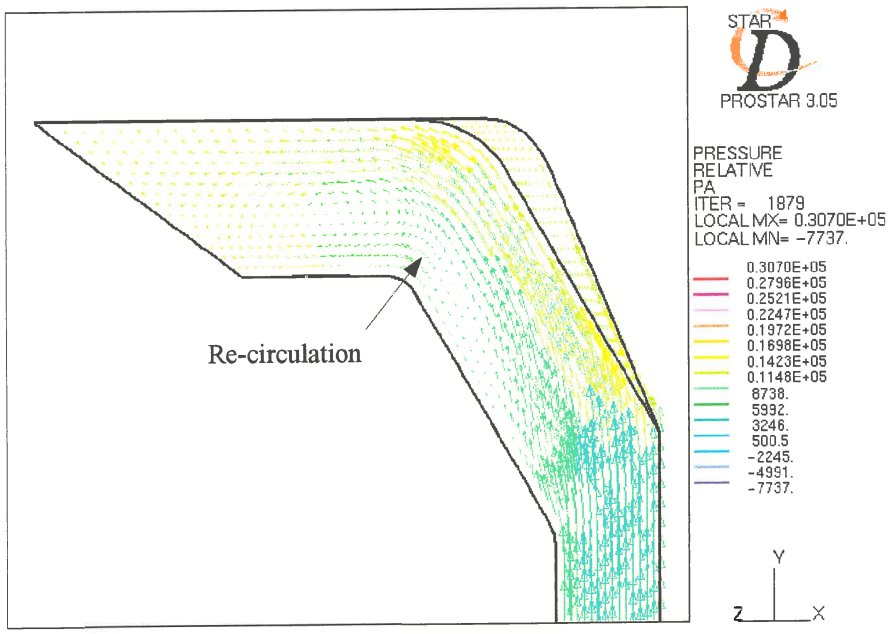

Figure E.18 Velocity vectors at outlet

Figures E.17 and E.18 show that the flow still gets separated at the outlet where a re-circulation region develops causing backward flow in the outlet. This will increase the damping. At the inlet (figure E.19) hardly any separation occurs.

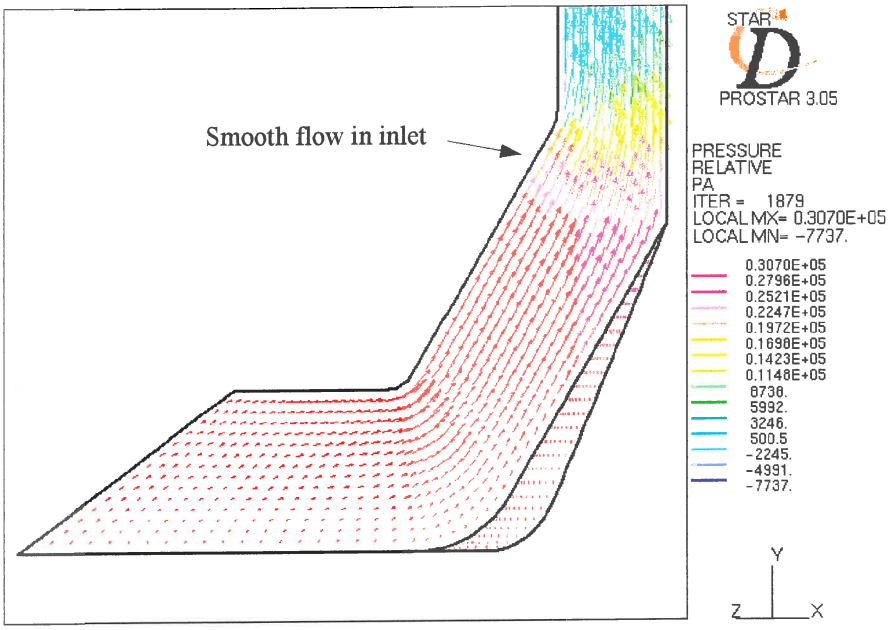

Figure E.19 Velocity vectors at inlet

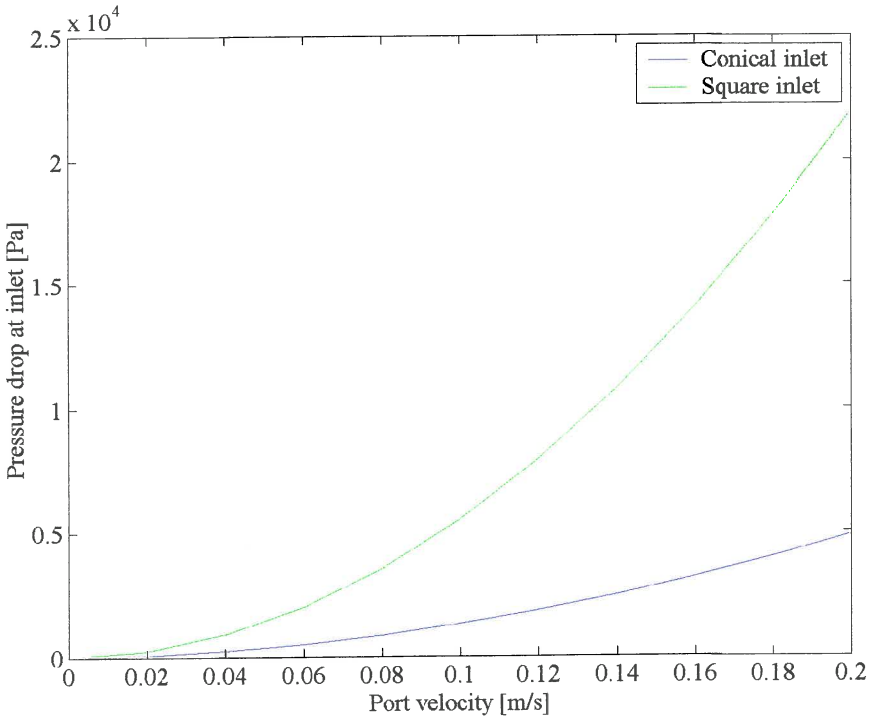

Figure E.20 The pressure drop at the inlet (Δp_o) as a function of port velocity ($\dot{x}$)

Figure E.20 shows that the pressure drop at the inlet is far less than for square inlets/outlets. The pressure drop decrease at the outlet is not as dramatic (figure E.21).

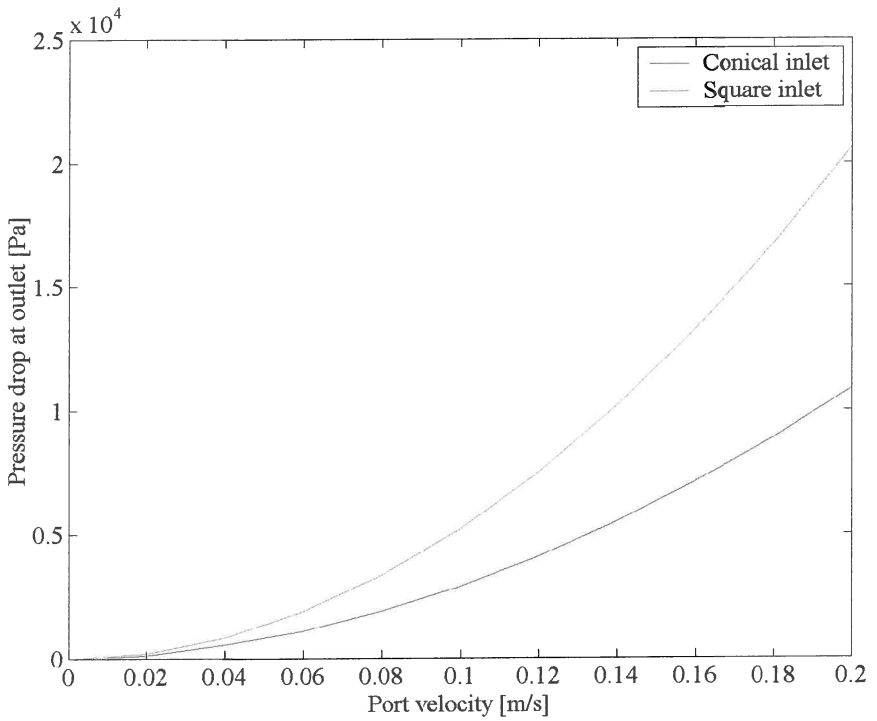

Figure E.21 The pressure drop at the outlet (Δp_o) as a function of port velocity ($\dot{x}$)

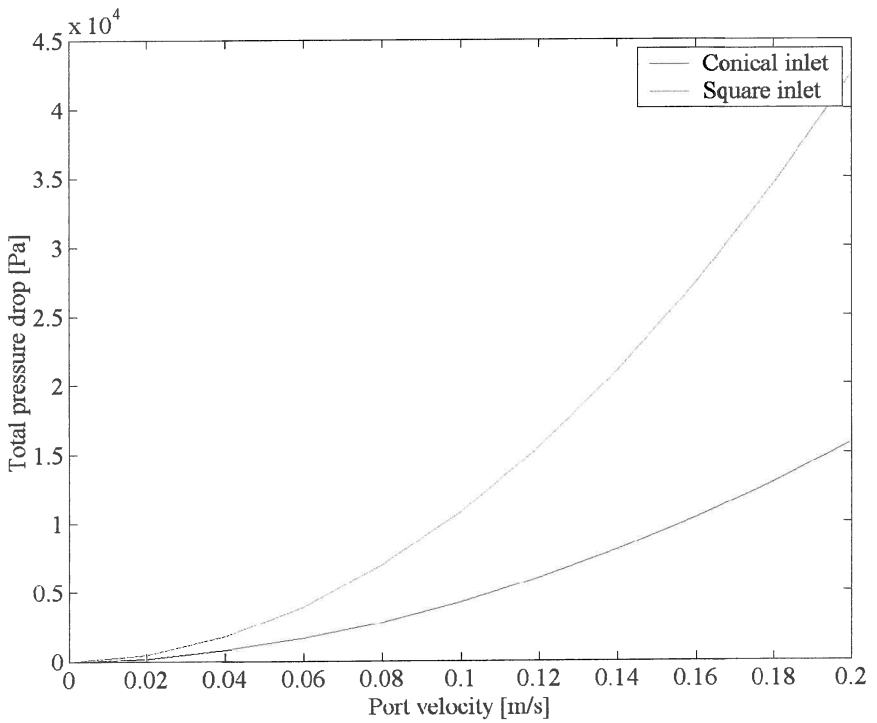

Figure E.22 Total pressure drop (Δp_i) as a function of port velocity ($\dot{x}$)

Figure E.22 shows that changes to the inlet/outlet geometry can have a major impact on the total pressure drop.

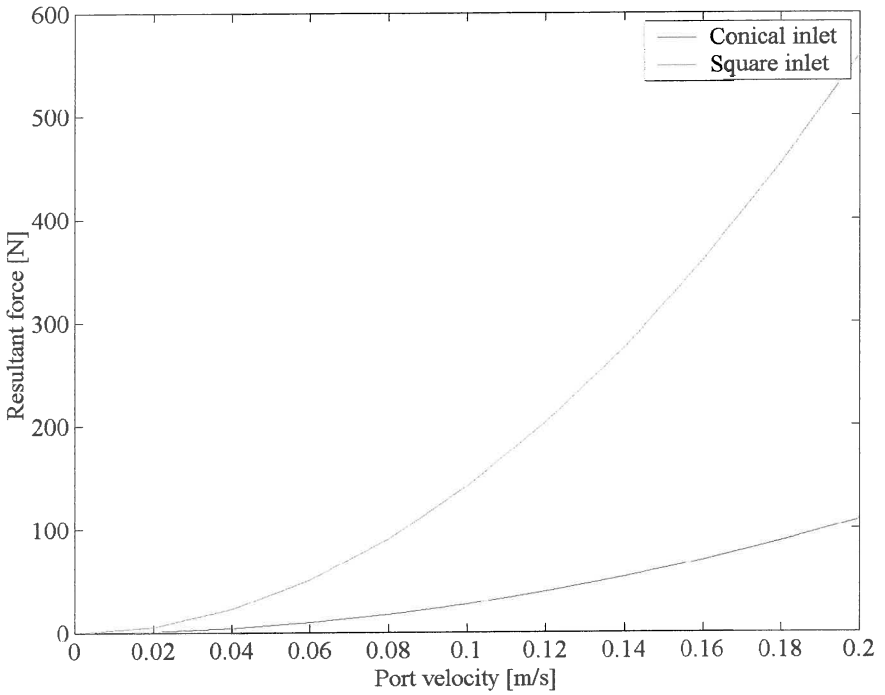

Figure E.23 Force in the z-direction (F_z) as a function of port velocity ($\dot{x}$)

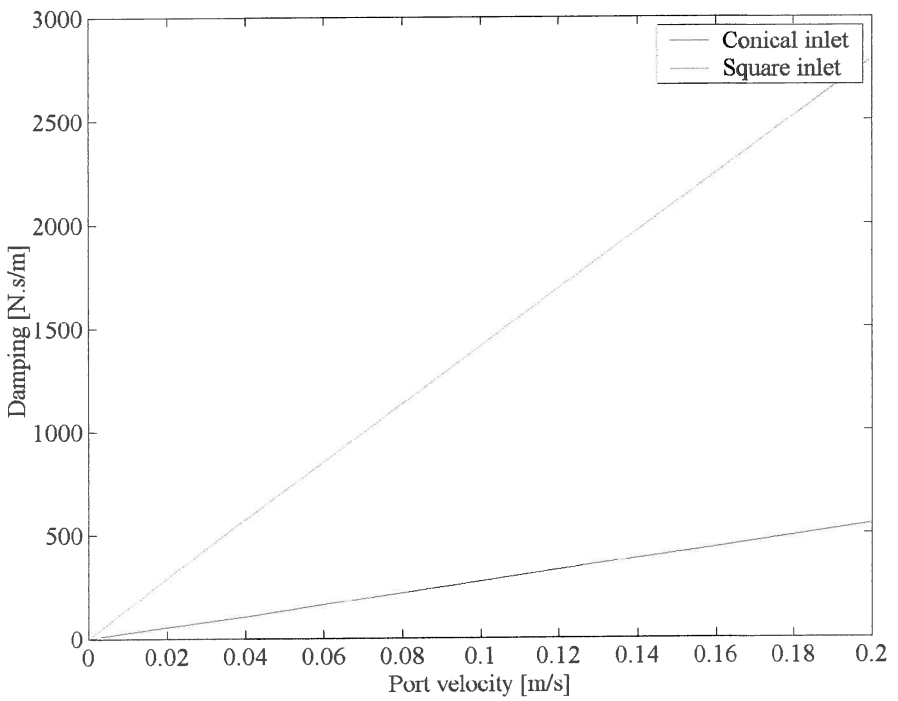

Figure E.24 Viscous damping (c) as a function of port velocity ($\dot{x}$)

The conical inlets/outlets reduced the viscous damping significantly as can be seen in figure E.24.

E.5. Conclusion

The CFD analysis proved to be worthwhile. The total pressure drop of the design is 2.5 times less than the theoretical model. The viscous damping coefficient is 5 times less. The design was done only with knowledge based on theory and empirical data and further improvements are therefore possible. Manufacturability also played a major role in the eventual choice of geometry. The port geometry can however be optimized using CFD. Optimization of the port geometry could significantly reduce damping further and is recommended for a future study.

APPENDIX F

Detail design

F.1. Component mass

Table F.1 Component mass

Item	#	Solid model [kg]	Actual [kg]
M14 threaded rod	2		0.00766
Lid	1	4.45	4.18
M8 allencap	6		0.02132
Washer	6		0.00125
Connector	1	17.6	16.98
Connector block 1	1	1.1	1.12
Connector block 2	1	1.1	1.10
M10 flat head socket screw	2		0.00234
M8 flat head socket screw	4		0.00186
Sleeve	1	8.41	7.92
O-ring	2		0.0036
Top plug	1	3.68	3.70
M6	1		0.0066
Washer	1		0.001
Spring	1	1.14	0.9
Port	1		4.74
Bottom plug	1	3.68	3.64

Table F.2 Volume

Item	Solid model [L]
Spring	1.071
Port	0.078
Reservoir	0.110
Total fluid	0.298

Table F.3 Density

	[kg/m^3]
Polyurethane	1060
Steel	7850
Water	1000

System mass 15.28 kg

F.2. Detail of the tuning port

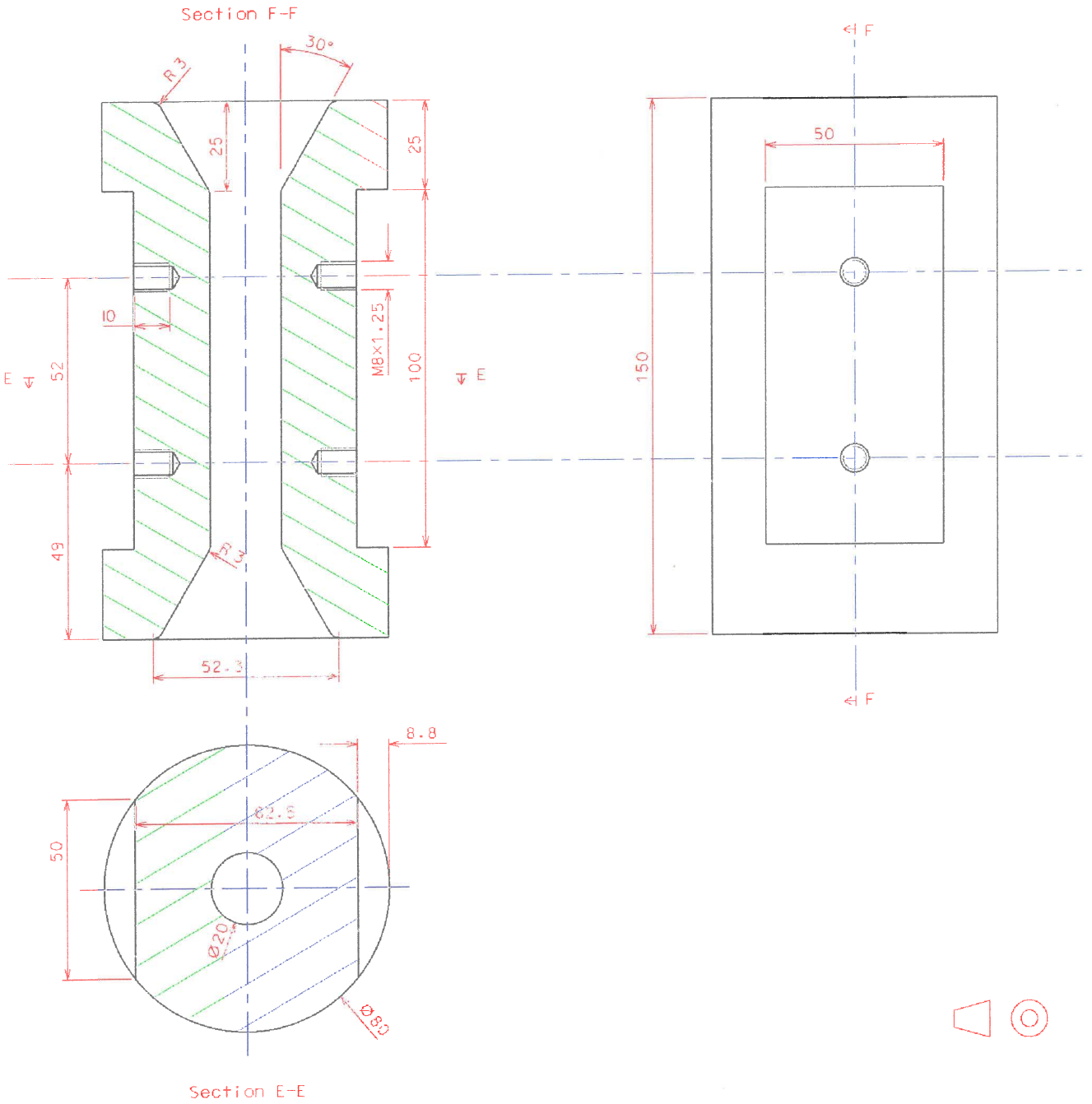

APPENDIX G

Test results of an absorber with a 55-Shore A spring

Table I.2. Test results for stiffness [MN/m].

	Hysteresis loop equation			Sine curve fit		
Frequency [Hz]	k_0	k_∞	$\Delta k/k_0$ [%]	k_0	k_∞	$\Delta k/k_0$ [%]
5	3.06	2.98	2.51	3.05	3.03	0.49
10	3.40	3.24	4.47	3.39	3.23	4.63
15	3.54	3.38	4.67	3.54	3.36	5.00
19	3.63	3.53	2.84	3.63	3.54	2.64
26	4.14	4.10	1.06	4.15	4.10	1.22
30	4.65	4.26	8.56	4.66	4.25	8.73
35	4.51	4.19	7.08	4.50	4.19	6.94
40	5.06	4.88	3.60	5.06	4.89	3.38

Curve fit not successful, $\Delta k = k_0 - k_\infty$

Table I.3. Average test results for stiffness [MN/m].

Frequency [Hz]	k_0	k_∞	$\Delta k/k_0$ [%]
5	3.05	3.01	1.50
10	3.39	3.24	4.55
15	3.54	3.37	4.83
19	3.63	3.53	2.74
26	4.15	4.10	1.14
30	4.66	4.25	8.64
35	4.50	4.19	7.01
40	5.06	4.88	3.49

Table I.4. Test results for the loss factor.

	Average peak method			Phase shift from curve fit			Energy method		
Frequency [Hz]	η_0	η_∞	$\Delta\eta/\eta_0$ [%]	η_0	η_∞	$\Delta\eta/\eta_0$ [%]	η_0	η_∞	$\Delta\eta/\eta_0$ [%]
5	0.27	0.27	1.78	0.28	0.27	4.42	0.34	0.32	4.31
10	0.42	0.40	2.98	0.42	0.41	3.79	0.46	0.45	3.02
15	0.48	0.47	1.73	0.49	0.48	2.39	0.51	0.50	1.70
19	0.50	0.50	0.62	0.50	0.50	1.38	0.53	0.51	3.15
26	0.53	0.52	2.33	0.53	0.53	-0.01	0.55	0.54	1.89
30	0.56	0.52	6.68	0.56	0.52	6.55	0.57	0.53	6.84
35	0.51	0.51	0.57	0.52	0.51	0.77	0.51	0.51	0.01
40	0.54	0.53	2.22	0.54	0.49	9.52	0.57	0.55	2.42

Curve fit not successful, $\Delta\eta = \eta_0 - \eta_\infty$

Table I.5. Average results for the loss factor.

	η_0	η_∞	$\Delta\eta/\eta_0$ [%]
5	0.30	0.29	3.57
10	0.43	0.42	3.26
15	0.49	0.48	1.94
19	0.51	0.50	1.74
26	0.53	0.53	1.41
30	0.56	0.52	6.69
35	0.51	0.51	0.45
40	0.55	0.52	4.70